

Screening in Hubbard models with long-range interactions

Florian Gebhard^{1*} and Kevin Bauerbach[†]

¹*Fachbereich Physik, Philipps-Universität Marburg, 35032 Marburg, Germany*

Örs Legeza^{2,3,4‡}

²*Strongly Correlated Systems Lendület Research Group,
Wigner Research Centre for Physics, P.O. Box 49, 1525 Budapest, Hungary*

³*Institute for Advanced Study, Technical University of Munich,
Lichtenbergstraße 2a, 85748 Garching, Germany and*

⁴*Parmenides Foundation, Hindenburgstraße 15, 82343, Pöcking, Germany*

(Dated: Polished version for PRB as of May 14, 2025)

We provide solid evidence for the long-standing presumption that model Hamiltonians with short-range interactions faithfully reproduce the physics of the long-range Coulomb interaction in real materials. For this aim, we address a generic Hubbard model that captures the quantum phase transitions between metal, Mott insulator, and charge-density-wave insulator, in the absence of Fermi-surface nesting. By comparing the quantum phase diagrams for the $1/r$ -Hubbard model on a half-filled chain with nearest-neighbor and $1/r$ -long-range interactions, we argue that the inclusion of long-range interactions is not crucial for a proper description of interacting many-electron systems. To this end, we employ the Density Matrix Renormalization Group method on finite lattices and antiperiodic boundary conditions to determine the quantum phase transitions between the metallic Luttinger liquid for weak interactions, the Mott-Hubbard insulator for dominant on-site interactions, and the charge-density wave insulator for dominant inter-site interactions. The two phase diagrams *qualitatively* agree inasmuch as the quantum phase transitions are continuous in both cases. Moreover, simple Hartree-Fock theory and the atomic limit provide renormalization factors that allow us to *quantitatively* map the two phase diagrams onto each other. As a practical advantage, our findings imply that computational efforts can be reduced tremendously by using models with short-range interactions only.

I. OVERVIEW

This overview introduces the reader to the fundamental issues, summarizes and illustrates our central results, and gives an outline to our work. After a brief introduction to the interacting-electron problem in Sect. IA, we present the quantum phase diagrams for the $1/r$ -Hubbard model with nearest-neighbor interaction and with $1/r$ -long-range interactions in Sect. IB. As central results of this work we show that the two phase diagrams agree qualitatively and that they can be mapped onto each other using simple renormalization factors that can be obtained from Hartree-Fock theory and the atomic limit. In the remainder of this work, as outlined in Sect. IC, we discuss the ground-state properties of the $1/r$ -Hubbard model with $1/r$ -long-range interactions that we obtain from using the numerical Density-Matrix Renormalization Group (DMRG) method.

A. Introduction

Electrons in a perfectly ordered solid at zero temperature pose a formidable quantum many-particle problem [1–3]. Modern-day computers can solve effective

single-particle problems to arbitrary accuracy so that Hartree(-Fock) calculations or density-functional theory provide relevant and reliable insight into the overall band structure. However, the single-particle picture cannot capture correlation effects, e.g., the correlation contribution to band gaps, or Mott insulating phases that arise due to the electron-electron interaction [4–7].

In the early 1960s, Hubbard [8] discussed a series of approximations to derive a model that still contains the essence of the electronic many-body problem. The Hubbard model, independently also introduced by Gutzwiller [9] and Kanamori [10], describes a single s -band of bandwidth W with nearest-neighbor electron transfers and purely on-site interactions of strength U between electrons of opposite spin orientation. Therefore, it disregards the complexity of multi-band systems and ignores the long-range nature of the Coulomb interaction. Due to these restrictions, the Hubbard model is often dismissed as a simplistic toy-model that has little relevance for real materials, if any.

Despite its conceptual simplicity, the Hubbard model captures essential correlation effects. For example, in finite dimensions it describes a continuous Mott transition at half band-filling as a function of U/W [11, 12], and also itinerant anti-ferromagnetism in single-band metals [6, 7, 13]. More specific features are not necessarily contained in the bare Hubbard model, such as excitons, i.e., bound electron-like and hole-like states in the optical excitation spectrum of an insulator. For the description of excitons in Mott insulators [14], the inclusion of

* florian.gebhard@physik.uni-marburg.de

† kevin.bauerbach@physik.uni-marburg.de

‡ legeza.ors@wigner.hu

a nearest-neighbor interaction of strength V_{NN} is mandatory ('extended Hubbard model' [6, 15, 16]).

The question remains whether or not the extended Hubbard model captures the essence of the long-range Coulomb interaction. For an electron and a hole, both short-range and long-range interactions can give rise to the formation of an exciton. However, the nature of the Mott transition could be altered because electrons in the metallic state screen the Coulomb interaction [1, 2] whereas the Coulomb interaction remains long-ranged at low energies in the insulating phase. Therefore, in the presence of long-range interactions the gap might open discontinuously as a function of the Coulomb parameters, in contrast to the case of the bare Hubbard model. In this work, we argue that the extended Hubbard model reproduces the quantum phase diagram of the Hubbard model with long-range Coulomb interactions.

It is very difficult to address these issues because the Hubbard model and its variants pose true many-particle problems that are unsolvable analytically, in general. An exception is one spatial dimension where the Bethe Ansatz provides exact results for the Hubbard model [12]. Unfortunately, in one spatial dimension the Mott transition generically occurs at $U = 0^+$ due to the nesting of the Fermi points [6, 11, 17]. Nesting is not prevalent in higher dimensions [18, 19]. Instead, the transition should generically occur when the Coulomb interaction is of the order of the bandwidth, $U_c \approx W$, in line with Mott's original arguments [4, 5]. Nesting can be avoided in one dimension when all electrons move in the same direction as is the case for the $1/r$ -Hubbard model with its linear dispersion relation, where the electron transfer amplitudes between sites decay proportional to the inverse of their distance r (' $1/r$ -Hubbard model'). In the absence of nesting, Umklapp scattering processes do not occur and the Mott transition is located at a finite interaction strength, $U_c = W$ for the $1/r$ -Hubbard model [6, 20, 21].

A number of exact results are known for the $1/r$ -Hubbard model that provide benchmark tests for the numerical density-matrix renormalization group (DMRG) method. It permits to study systems with up to $L = 64$ lattice sites and periodic boundary conditions so that reliable results can be obtained from extrapolations to the thermodynamic limit [22]. Using DMRG we obtained the quantum phase diagram for the extended $1/r$ -Hubbard model [23]. In this work, we derive the zero-temperature phase diagram for the $1/r$ -Hubbard model with $1/r$ -long-range interactions. Our comparison shows no qualitative differences. Moreover, we can map the two phase diagrams onto each other quantitatively using simple renormalization factors that we derive from bare Hartree-Fock theory and the atomic limit, respectively.

B. Phase diagrams

In Fig. 1a we recall the quantum phase diagram of the $1/r$ -Hubbard model with repulsive nearest-neighbor

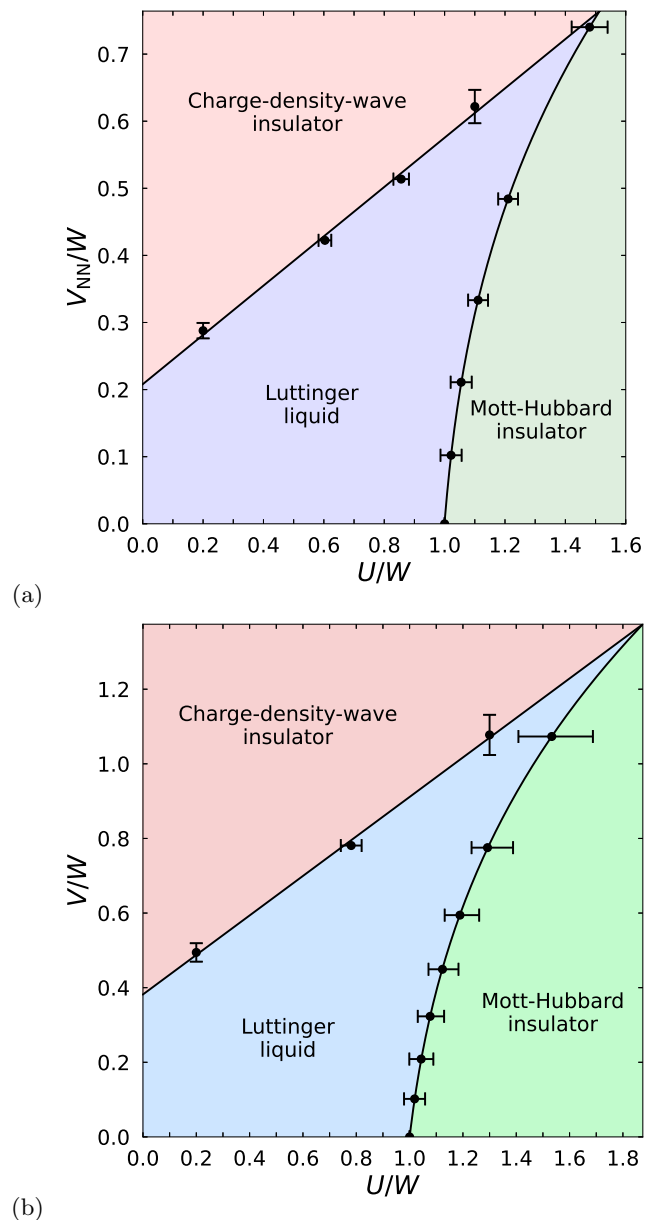


Figure 1. (a) Phase diagram of the one-dimensional $1/r$ -Hubbard model with nearest-neighbor interactions V_{NN} . (b) Phase diagram of the one-dimensional $1/r$ -Hubbard model with $1/r$ -long-range interactions. Dots: estimate for the critical interaction, \overline{U}_c , with error bounds; continuous lines: polynomial fits, see Sect. V.

interactions [23]. As can be argued using perturbation theory, the metallic Luttinger liquid appears in the region of weak interactions ($W \gg U, V_{\text{NN}}$), the Mott-Hubbard insulator is found for dominant Hubbard interactions ($U \gg W, V_{\text{NN}}$), and the charge-density-wave (CDW) phase occurs for dominant inter-site interactions ($V_{\text{NN}} \gg W, U$).

For dominant Coulomb interactions, the separation line between the Mott-Hubbard insulator and the CDW

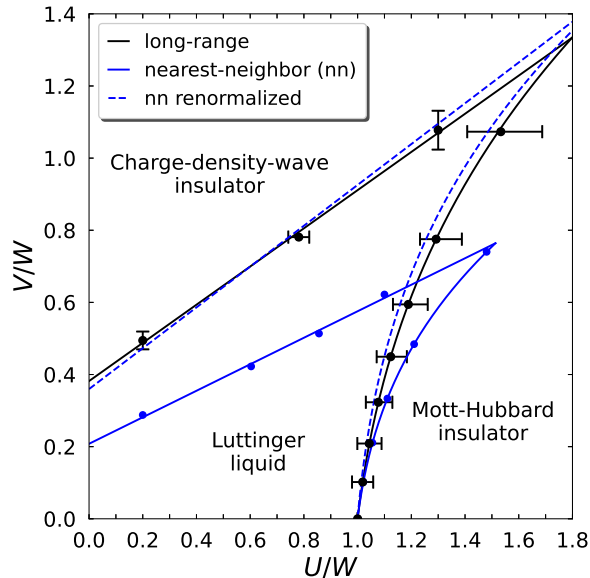


Figure 2. Renormalized phase diagram. The phase separation lines of the $1/r$ -Hubbard model with $1/r$ -long-range interactions (black solid line) and nearest-neighbor interactions (blue solid line) can be mapped onto each other using $V_{\text{NN}} = R_{\text{qp}} V_{\text{LR}}$ with $R_{\text{CDW}} = 0.606$ and $R_{\text{Mott}} = \ln 2 \approx 0.693$ for the CDW and Mott quantum phase transitions. The renormalized quantum phase transition lines for the extended $1/r$ -Hubbard model (dashed blue lines) reproduce those of the $1/r$ -Hubbard model with $1/r$ -long-range interactions (black solid lines) within error bars.

insulator is given by $V_{\text{NN}} = U/2$ to leading order, with a stabilization tendency toward the Mott-Hubbard insulator in the next order in $1/U$.

In the absence of inter-site interactions, the Mott-Hubbard transition occurs at $U_c(V=0) = W$ [6, 20, 22]. The inclusion of a repulsive nearest-neighbor interaction stabilizes the metallic phase because the additional repulsive interaction softens the two-particle scattering potential in position space.

For comparison, in Fig. 1b, we show the quantum phase diagram of the $1/r$ -Hubbard model with repulsive inter-site interactions that decay proportional to V_{LR}/r ($1/r$ -long-range interactions). As our first main result, we see that the quantum phase diagrams agree *qualitatively*. Both the Mott and CDW transitions remain *continuous* even in the presence of $1/r$ -long-range interactions.

The agreement can be made *quantitative* within error bounds by using simple renormalization factors, see Fig. 2. This approximate yet quantitatively satisfactory mapping procedure is our second main result.

The phase diagrams are characterized by phase separation lines. For $V > V_c^{\text{CDW}}(U)$ the CDW insulator is stable, whereas the Mott-Hubbard insulator prevails for $U > U_c^{\text{Mott}}(V) \geq 1$ when $0 \leq V \leq V_c^{\text{CDW}}(U)$.

For small interactions, Hartree-Fock theory predicts $V_{c,\text{NN}}^{\text{CDW}}(0)/V_{c,\text{LR}}^{\text{CDW}}(0) \approx R_{\text{HF}}^{\text{CDW}}(0) = 0.606$, see appendix, which we use to renormalize the CDW critical line by $V_{\text{NN}} = R_{\text{CDW}} V_{\text{LR}}$, $R_{\text{CDW}} = 0.61$.

On the other hand, in the atomic limit, the CDW and Mott-Hubbard insulators are separated by $V_c^{\text{CDW}}(U) = U/(2 \ln(2)) \approx 0.721U$ for the $1/r$ -Hubbard model with $1/r$ -long-range interactions, see appendix. Thus, the renormalization factor in the atomic limit is given by $R_{\text{Mott}}^{\text{al}} = (1/2)/[1/(2 \ln 2)] = \ln 2 \approx 0.693$. In Fig. 2, the Mott critical lines $U_c^{\text{Mott}}(V)$ of the $1/r$ -Hubbard models with nearest-neighbor and $1/r$ -long-range interactions are then mapped onto each other using $V_{\text{NN}} = R_{\text{Mott}} V_{\text{LR}}$, $R_{\text{Mott}} = 0.69$.

The successful mapping indicates that the $1/r$ -long-range interaction of strength V_{LR} in one dimension can be replaced by a nearest-neighbor interaction V_{NN} that is smaller by a factor $R \approx 2/3$, $V_{\text{NN}} \approx R V_{\text{LR}}$.

Before we proceed, we caution the reader that our findings relate to the ground-state and low-energy physics of interacting quantum particles. It is well known that an attractive potential well can be used to describe semi-quantitatively the $1s$ bound state of the hydrogen atom or of an exciton. However, such an approach fails to describe properly the fine structure of the wave functions or the energy of higher-excited states. Similarly, the long-range tail of the Coulomb interaction can give rise to exotic phenomena, particularly under non-equilibrium conditions. Long-range interactions are also more significant in dilute bosonic systems, see the example of polar bosonic gases in one-dimensional lattice [24], or in the case of bosonic many-body localization [25], and references therein.

C. Outline

For better comparability, we closely follow the structure of our previous publication [23]. Therefore, we start in Sect. II with the definition of the Hubbard model with $1/r$ -long-range electron transfers as well as on-site and $1/r$ -long-range Coulomb interactions. We introduce the ground-state properties of interest, namely, the ground-state energy, the two-particle gap, the momentum distribution, and the density-density correlation function from which we determine the Luttinger parameter in the metallic phase and the charge-density-wave (CDW) order parameter.

In Sect. III we present results for the ground-state properties. In addition, we discuss their finite-size dependencies and extrapolations to the thermodynamic limit where appropriate.

In Sect. IV we focus on the Mott transition in the presence of long-range interactions between electrons on different lattice sites. We propose and discuss several methods to extract the critical interaction strength for the Mott-Hubbard transition based on the ground-state energy, the two-particle gap, the Luttinger parameter, and

the structure factor, whereby we study the Mott transition at fixed $v \equiv V_{\text{LR}}/U$ in the range $0 \leq v \leq 0.7$ with increment $\Delta v = 0.1$, in units of the bandwidth, $W \equiv 1$. Moreover, we address the transition to the CDW insulator in the presence of long-range interactions, which can be determined using the CDW order parameter and the Luttinger parameter. We study this transition for a fixed ratio $v = V_{\text{LR}}/U = 1$, as well as for fixed values of $U = 0.2$ and $U = 1.3$.

In Sect. V, we present and discuss the complete phase diagram for the model with long-range interactions. We compare it in detail with the phase diagram of the extended Hubbard model which contains only on-site and nearest-neighbor interactions. In addition, we introduce a method to quantitatively map the two quantum phase diagrams onto each other.

In our conclusions, Sect. VI, we summarize our findings and discuss their relevance in a broader context. Hartree-Fock calculations for the CDW transition are collected in the appendix.

II. 1/ r -HUBBARD MODEL

A. Hamiltonian

In this work, we address the one-dimensional single-band 1/ r -Hubbard model [6] with on-site ($U\hat{D}$) and long-range interactions ($V\hat{V}$)

$$\hat{H} = \hat{T} + U\hat{D} + V\hat{V} \quad (1)$$

on a ring with L sites; L is even. For convenience, we abbreviate $V \equiv V_{\text{LR}}$. We discuss the kinetic energy and the Coulomb interaction terms separately.

1. Kinetic energy

The kinetic energy describes the tunneling of electrons with spin $\sigma = \uparrow, \downarrow$ along a ring with L sites,

$$\hat{T} = \sum_{\substack{l,m=1 \\ l \neq m; \sigma}}^L t(l-m) \hat{c}_{l,\sigma}^\dagger \hat{c}_{m,\sigma} . \quad (2)$$

The creation and annihilation operators $\hat{c}_{l,\sigma}^\dagger$, $\hat{c}_{l,\sigma}$ for an electron with spin $\sigma = \uparrow, \downarrow$ on lattice site l obey the usual anti-commutation relations for fermions.

In this work, we focus on the 1/ r -Hubbard model for which the electron transfer between lattice sites is defined by

$$\begin{aligned} t(r) &= (-it) \frac{(-1)^r}{d(r)} , \\ d(r) &= \frac{L}{\pi} \sin\left(\frac{\pi r}{L}\right) . \end{aligned} \quad (3)$$

Here, $d(l-m)$ is the chord distance between the sites l and m on a ring. In the thermodynamic limit and for $|l-m| \ll L$ fixed, we have $d(l-m) = (l-m) + \mathcal{O}(1/L^2)$, and the electron transfer amplitude between two sites decays inversely proportional to their distance ('1/ r -Hubbard model').

Since L is even, we have anti-periodic electron transfer amplitudes because $d(L+r) = -d(r)$. Therefore, we choose anti-periodic boundary conditions

$$\hat{c}_{L+l,\sigma} = -\hat{c}_{l,\sigma} \quad (4)$$

for the operators, too. Under these boundary conditions, the kinetic energy operator becomes diagonal in Fourier space,

$$\begin{aligned} \hat{C}_{k,\sigma}^+ &= \frac{1}{\sqrt{L}} \sum_{l=1}^L e^{ikl} \hat{c}_{l,\sigma}^+ , \\ \hat{c}_{l,\sigma}^+ &= \frac{1}{\sqrt{L}} \sum_k e^{-ikl} \hat{C}_{k,\sigma}^+ , \\ k &= \frac{(2m+1)\pi}{L} , \quad m = -\frac{L}{2}, \dots, \frac{L}{2} - 1 , \end{aligned} \quad (5)$$

so that

$$\hat{T} = \sum_{k,\sigma} \epsilon(k) \hat{C}_{k,\sigma}^+ \hat{C}_{k,\sigma} . \quad (6)$$

The dispersion relation of the 1/ r -Hubbard model is linear, $\epsilon(k) = tk$. We set $t = 1/(2\pi)$ for a unit bandwidth, $W \equiv 1$.

In this work, we focus on the case of a paramagnetic half-filled ground state where we have the same number of electrons per spin species, $N_\uparrow = N_\downarrow$, that equals half the number of lattice sites, $N_\sigma = L/2$ ($\sigma = \uparrow, \downarrow$).

2. Coulomb interaction

The Coulomb interaction is parameterized by two terms in Eq. (1). The on-site (Hubbard) interaction [8–10] acts locally between two electrons with opposite spins,

$$\hat{D} = \sum_{l=1}^L \hat{n}_{l,\uparrow} \hat{n}_{l,\downarrow} , \quad \hat{n}_{l,\sigma} = \hat{c}_{l,\sigma}^\dagger \hat{c}_{l,\sigma} , \quad (7)$$

where $\hat{n}_{l,\sigma}$ counts the number of electrons with spin σ on site l , and $\hat{n}_l = \hat{n}_{l,\uparrow} + \hat{n}_{l,\downarrow}$ counts the number of electrons on site l . The corresponding operators for the total number of electrons with spin $\sigma = \uparrow, \downarrow$ are denoted by $\hat{N}_\sigma = \sum_l \hat{n}_{l,\sigma}$, and $\hat{N} = \hat{N}_\uparrow + \hat{N}_\downarrow$.

To discuss the influence of the extended nature of the Coulomb interaction, we consider

$$\begin{aligned} \hat{V} &= \sum_{r=1}^{L/2} V(r) \sum_{l=1}^L (\hat{n}_l - 1)(\hat{n}_{l+r} - 1) , \\ V(r) &= \frac{1}{d(r)} \end{aligned} \quad (8)$$

with $d(r)$ from Eq. (3). Due to the ring geometry, we limit ourselves to distances $1 \leq r \leq L/2$.

For comparison, we shall also show results for the extended $1/r$ -Hubbard model, $V(r) = \delta_{r,1}$, as collected in Ref. [23].

3. Particle-hole symmetry

We study the case of an anti-symmetric dispersion relation where $t(-r) = -t(r)$. Under the particle-hole transformation

$$\hat{c}_{l,\sigma} \mapsto \hat{c}_{l,\sigma}^+ \quad , \quad \hat{n}_{l,\sigma} \mapsto 1 - \hat{n}_{l,\sigma} \quad , \quad (9)$$

the kinetic energy remains unchanged,

$$\begin{aligned} \hat{T} &\mapsto \sum_{\substack{l,m=1 \\ l \neq m; \sigma}}^L t(l-m) \hat{c}_{l,\sigma}^+ \hat{c}_{m,\sigma}^+ \\ &= \sum_{\substack{l,m=1 \\ l \neq m; \sigma}}^L [-t(m-l)] \hat{c}_{l,\sigma}^+ \hat{c}_{m,\sigma} = \hat{T} \end{aligned} \quad (10)$$

because $t(-r) = -t(r)$. Furthermore,

$$\hat{D} \mapsto \sum_{l=1}^L (1 - \hat{n}_{l,\uparrow})(1 - \hat{n}_{l,\downarrow}) = \hat{D} - \hat{N} + L \quad , \quad (11)$$

and

$$\hat{V} \mapsto \hat{V} \quad . \quad (12)$$

Therefore, $\hat{H}(N_\uparrow, N_\downarrow)$ has the same spectrum as $\hat{H}(L - N_\uparrow, L - N_\downarrow) - U(2L - N) + LU$, where $N = N_\uparrow + N_\downarrow$ is the particle number.

B. Ground-state properties

The interplay between long-range interactions $V\hat{V}$, on-site (Hubbard) interactions $U\hat{D}$, and the fermions' kinetic energy \hat{T} , characterized by the bandwidth W , gives rise to a complex quantum phase diagram at half band-filling, $n = N/L = 1$. We are interested in the metal-insulator transition where the metallic Luttinger liquid for weak interactions, $U, V \ll W$, turns into a paramagnetic Mott-Hubbard insulator for large on-site interactions at some finite value $U_c^{\text{Mott}}(V)$ for $U \gg W, V$, or to a charge-density wave insulator at $V_c^{\text{CDW}}(U)$ for strong inter-site interactions, $V \gg U, W$.

For the $1/r$ -Hubbard model, metal-insulator transitions can be determined through finite-size extrapolation of both the ground-state energy and the two-particle gap [22, 23]. Alternatively, the Luttinger parameter [26] and the finite-size extrapolation of the structure factor at the Brillouin zone boundary provide a way to identify the critical interaction strength. Additionally, the

charge-density-wave state can be characterized using the CDW order parameter.

In this section, we also present results for the momentum distribution for finite systems, which can be obtained via DMRG [27, 28].

1. Ground-state energy and two-particle gap

We denote the ground-state energy by

$$E_0(N, L; U, V) = \langle \Psi_0 | \hat{H} | \Psi_0 \rangle \quad (13)$$

for given particle number N , system size L , and interaction parameters U, V . Here, $|\Psi_0\rangle$ is the normalized ground state of the Hamiltonian (1). We are interested in the thermodynamic limit, $N, L \rightarrow \infty$ with $n = N/L$ fixed. We denote the ground-state energy per site and its extrapolated value by

$$\begin{aligned} e_0(N, L; U, V) &= \frac{1}{L} E_0(N, L; U, V) \quad , \\ e_0(n; U, V) &= \lim_{L \rightarrow \infty} e_0(N, L; U, V) \quad , \end{aligned} \quad (14)$$

respectively.

The two-particle gap is defined by

$$\Delta_2(L; U, V) = \mu_2^+(L; U, V) - \mu_2^-(L; U, V) \quad , \quad (15)$$

where

$$\begin{aligned} \mu_2^-(L; U, V) &= E_0(L, L; U, V) - E_0(L-2, L; U, V) \quad , \\ \mu_2^+(L; U, V) &= E_0(L+2, L; U, V) - E_0(L, L; U, V) \end{aligned} \quad (16)$$

are the chemical potentials for adding the last two particles to achieve half filling and the first two particles beyond half filling, respectively.

Due to particle-hole symmetry, we have

$$\mu_2^-(L; U, V) = 2U - \mu_2^+(L; U, V) \quad (17)$$

so that

$$\Delta_2(L; U, V) = 2\mu_2^+(L; U, V) - 2U \quad (18)$$

and

$$\Delta_2(U, V) = \lim_{L \rightarrow \infty} \Delta_2(L; U, V) \quad (19)$$

in the thermodynamic limit. We always consider the spin symmetry sector $S = S^z = 0$. For this reason, we study the two-particle gap rather than the single-particle gap.

The two added particles repel each other so that, in the thermodynamic limit, they are infinitely separated from each other. Therefore, we have

$$\Delta_2(U, V) = 2\Delta_1(U, V) \quad , \quad (20)$$

where $\Delta_1(U, V)$ is the gap for single-particle excitations. For finite systems, we expect the interaction energy

$$e_R(L; U, V) = \Delta_2(L; U, V) - 2\Delta_1(L; U, V) = \mathcal{O}(1/L) > 0 \quad (21)$$

to be positive, of the order $1/L$. We verified that the interaction energy vanishes in the thermodynamic limit for the case $V = 0$ [22].

2. Momentum distribution

We also study the spin-summed momentum distribution in the ground state at half band-filling, $N = L$,

$$\begin{aligned} n_k(L; U, V) &= \langle \Psi_0 | \hat{n}_{k,\uparrow} + \hat{n}_{k,\downarrow} | \Psi_0 \rangle \\ &= \sum_{l,m;\sigma} e^{ik(l-m)} P_{l,m;\sigma} \end{aligned} \quad (22)$$

with $\hat{n}_{k,\sigma} = \hat{C}_{k,\sigma}^\dagger \hat{C}_{k,\sigma}$ and the single-particle density matrix $P_{l,m;\sigma} = \langle \Psi_0 | \hat{c}_{l,\sigma}^\dagger \hat{c}_{m,\sigma} | \Psi_0 \rangle$. Due to particle-hole symmetry, we have

$$n_k(L; U, V) = 1 - n_{-k}(L; U, V) \quad (23)$$

at half band-filling. Therefore, it is sufficient to study wave numbers from the interval $-\pi < k < 0$.

3. Density-density correlation function and Luttinger parameter

Lastly, we address the density-density correlation function at half band-filling, $N = L$,

$$C^{\text{NN}}(r, L; U, V) = \frac{1}{L} \sum_{l=1}^L (\langle \hat{n}_{l+r} \hat{n}_l \rangle - \langle \hat{n}_{l+r} \rangle \langle \hat{n}_l \rangle), \quad (24)$$

where $\langle \dots \rangle \equiv \langle \Psi_0 | \dots | \Psi_0 \rangle$. The limit $L \gg r \gg 1$ for $U, V \ll W$ is also accessible from field theory [17, 29, 30],

$$C^{\text{NN}}(r \gg 1; U, V) \sim -\frac{K(U, V)}{(\pi r)^2} + \frac{A(U, V)(-1)^r}{r^{1+K}[\ln(r)]^{3/2}} + \dots, \quad (25)$$

where $A(U, V)$ is a constant that depends on the interaction but not on the distance r .

We extract the Luttinger parameter $K(U, V)$ from the structure factor,

$$\tilde{C}^{\text{NN}}(q, L; U, V) = \sum_{r=0}^{L-1} e^{-iqr} C^{\text{NN}}(r, L; U, V), \quad (26)$$

where the wave numbers are from momentum space, $q = (2\pi/L)m_q$, $m_q = -L/2, -L/2 + 1, \dots, L/2 - 1$. By construction, $\tilde{C}^{\text{NN}}(q = 0, L; U, V) = 0$ because the particle number is fixed, $N = L$ in the half-filled ground state. In the thermodynamic limit, the structure factor $\tilde{C}^{\text{NN}}(q, L; U, V)$ remains of the order unity even in

the CDW phase because we subtract the contributions of the long-range order in the definition (24).

The transition to a charge-density-wave insulator can be monitored from the CDW order parameter. In this work, we do not study the standard CDW order parameter,

$$D(L; U, V) = \frac{1}{L} \left| \sum_{r=0}^{L-1} (-1)^r (\langle \hat{n}_r \rangle - 1) \right| \leq 1. \quad (27)$$

Instead, we include all short-range contributions and address

$$N_\pi(L; U, V) = \frac{1}{L} \sum_{r=0}^{L-1} (-1)^r \frac{1}{L} \sum_{l=0}^{L-1} (\langle \hat{n}_{r+l} \hat{n}_l \rangle - 1). \quad (28)$$

When the charges are homogeneously distributed, $\langle \hat{n}_l \rangle = 1$, we have $N_\pi(L; U, V) = \tilde{C}^{\text{NN}}(\pi, L; U, V)/L$, and the order parameter vanishes in the metallic phase. More generally, in the thermodynamic limit we have $N_\pi(U, V) = (D(U, V))^2$. In the $1/r$ -Hubbard model with its long-range electron transfer, it is advantageous to analyze $N_\pi(L; U, V)$ to facilitate a reliable finite-size analysis.

When Eq. (25) is employed, it follows that the Luttinger parameter for finite systems,

$$K(L; U, V) = \frac{L}{2} \tilde{C}^{\text{NN}}(2\pi/L, L; U, V), \quad (29)$$

can be used to calculate the Luttinger parameter in the thermodynamic limit,

$$\begin{aligned} K(U, V) &= \lim_{L \rightarrow \infty} K(L; U, V) \\ &= \pi \lim_{q \rightarrow 0} \frac{\tilde{C}^{\text{NN}}(q; U, V)}{q}, \end{aligned} \quad (30)$$

where we denote the structure factor in the thermodynamic limit by $\tilde{C}^{\text{NN}}(q; U, V)$. Using Eq. (30), the Luttinger parameter can be calculated numerically with very good accuracy [31]. The Luttinger parameter can be used to locate the metal-insulator transition in one dimension.

III. GROUND-STATE PROPERTIES

Before we investigate the Mott transition for the half-filled $1/r$ -Hubbard model with $1/r$ -long-range interactions in more detail in the next section, we present DMRG results for the ground-state energy, the two-particle gap, the momentum distribution, the structure factor, and the CDW order parameter. For the numerical calculations we employ the same high accuracy SU(2) spin adapted DMRG code as for our previous work [22, 23] with bond dimension $D_{\text{SU}(2)}$ up to $D_{\text{SU}(2)}^{\text{max}} = 6000$.

A. Ground-state energy

For $V = 0$, the ground-state energy per site for finite system sizes is given by ($n = N/L$, N : even) [6, 20, 22]

$$e_0 = \frac{1}{4}n(n-1) + \frac{U}{4}n - \frac{1}{2L} \sum_{r=0}^{(N/2)-1} \sqrt{1 + U^2 - 4U(2r+1 - L/2)/L} \quad (31)$$

with the abbreviation $e_0 \equiv e_0(N, L; U, V = 0)$.

In the thermodynamic limit at $n = 1$, the ground-state energy per site becomes particularly simple,

$$\begin{aligned} e_0(n=1; U \leq 1, V=0) &= -\frac{1}{4} + \frac{U}{4} - \frac{U^2}{12}, \\ e_0(n=1; U \geq 1, V=0) &= -\frac{1}{12U}. \end{aligned} \quad (32)$$

The analytic expressions (31) and (32) are useful for a comparison with numerical data at $V = 0$.

For finite V , we can use first-order perturbation theory for weak interactions, $U, V \ll 1$, and at half band-filling to find

$$e_0^{\text{PT}}(U, V) = -\frac{1}{4} + \frac{U}{4} \left(1 - \frac{8v}{\pi^2} \frac{7\zeta(3)}{8} \right) + \mathcal{O}(U^2) \quad (33)$$

with $v = V/U$ in the thermodynamic limit and $\zeta(x)$ is the Riemann zeta function. Note that Eq. (33) holds for all v , as long as $U, V \ll 1$.

We display the ground-state energy per site at half band-filling, $e_0(L, L; U, V)$, as a function of the inverse system size ($L = 8, 16, 24, 32, 48, 64$) and various values of U in Fig. 3a ($v = 0.1$), Fig. 3b ($v = 0.3$), and Fig. 3c ($v = 0.5$). For the extrapolation to the thermodynamic limit, we use the algebraic fit function

$$e_0(L, L; U, V) = e_0(n=1; U, V) + a_0(U, V) \left(\frac{1}{L} \right)^{\gamma_0(U, V)}, \quad (34)$$

where $e_0(n=1; U, V)$ denotes the numerical estimate for the ground-state energy density in the thermodynamic limit; $a_0(U, V)$ and $\gamma_0(U, V)$ are the two other fit parameters. This extrapolation scheme is appropriate for $V = 0$ [22] because the ground-state energy per site scales with $(1/L)^2$ for $U \neq 1$ and with $(1/L)^{3/2}$ for $U = U_c(V=0) = 1$, as follows from Eq. (31).

More generally, we *assume* for all (U, V)

$$\gamma_0(U, V) = \begin{cases} 2 & \text{for } U \neq U_c(V) \\ 3/2 & \text{for } U = U_c(V) \end{cases}. \quad (35)$$

Eq. (35) follows from the fact that the ground-state energy density displays generic $(1/L)^2$ finite-size corrections when the model is not critical. When the holon dispersion displays a square-root divergence at low energies for

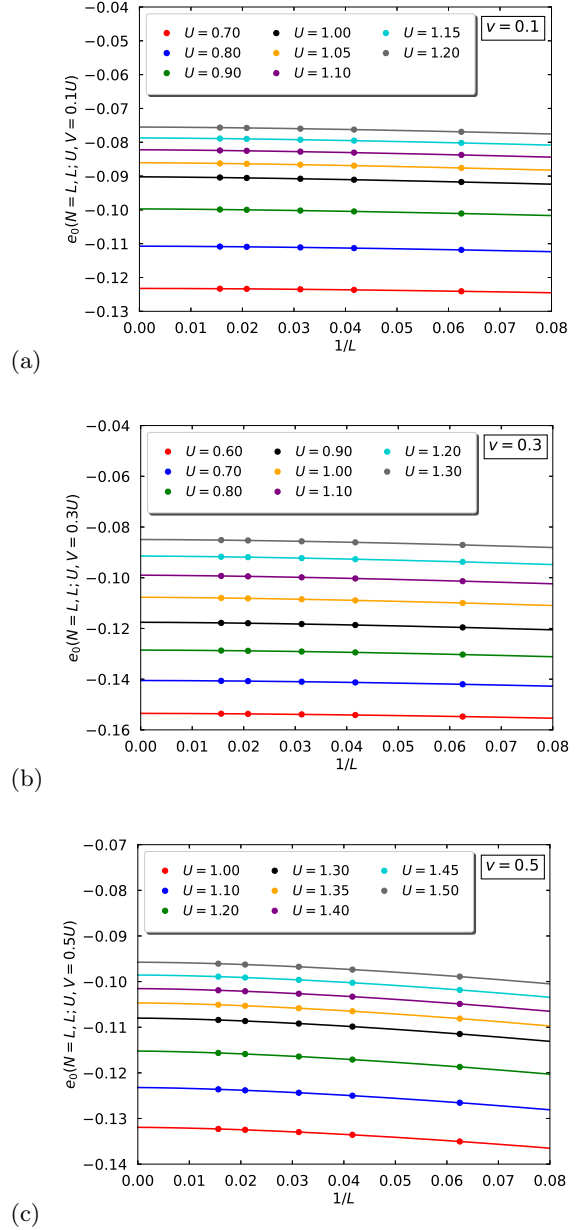


Figure 3. Ground-state energy per lattice site at half band-filling, $e_0(N = L, L; U, V)$, for the $1/r$ -Hubbard model with $1/r$ -long-range interactions as a function of $1/L$ for $L = 8, 16, 24, 32, 48, 64$ and various values for U for (a) $v = 0.1$, (b) $v = 0.3$, (c) $v = 0.5$. The continuous lines are fits to the algebraic fit function (34). The intercept of the extrapolation curves with the ordinate defines the extrapolation estimate $e_0(n=1; U, V)$ in the thermodynamic limit.

$U_c(V)$, the exponent is reduced to $\gamma_0(U_c(V), V) = 3/2$, as in the case of the bare $1/r$ -Hubbard model. We shall discuss the finite-size modifications in detail in Sec. IV.

The extrapolated ground-state energies are shown in Fig. 4 for $1/r$ -long-range interactions (crosses) and for nearest-neighbor interactions (open triangles), together with the exact result for $V = 0$. For small interactions,

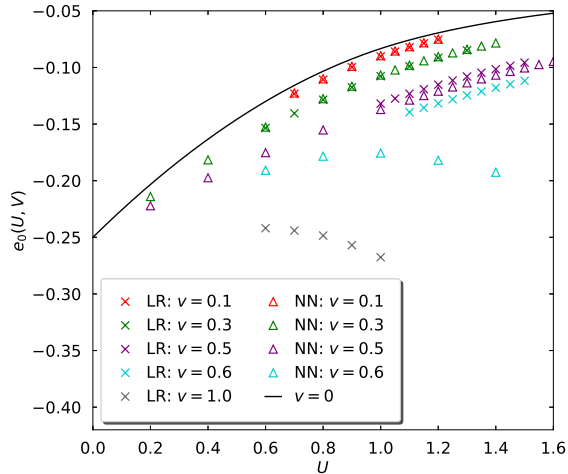


Figure 4. Ground-state energy density at half band-filling, $e_0(n=1; U, V)$, for the $1/r$ -Hubbard model with $1/r$ -long-range interactions (crosses) from the extrapolation to the thermodynamic limit in Fig. 3, and for the extended $1/r$ -Hubbard model (open triangles, see Ref. [23]). The continuous line is the exact result for $V=0$, $e_0(n=1; U, V=0)$.

the long-range interactions in the particle-hole symmetric form decrease the ground-state energy because the Hartree contribution at half band-filling is subtracted in the definition of the interaction, and the Fock contribution is negative because of the exchange hole. Therefore, the linear term in the interaction $(U/4)(1 - 7v\zeta(3)/\pi^2)$, see Eq. (33), is smaller in the presence of repulsive long-range interactions.

At large interactions, the ground-state energy approaches zero, $\lim_{U \rightarrow \infty} e_0(n=1; U, V=vU) = 0$, as long as the charge-density wave is absent. In the presence of a CDW, the ground-state energy is negative and proportional to U for large interactions, $e_0(U \gg 1, V) = U(1/2 - v \ln 2)$, see appendix. Therefore, the ground-state energy displays a maximum for $v \gtrsim 1$ because its slope as a function of U is positive for small interactions and negative for large interaction strengths in the CDW phase. This result further demonstrates that as soon as the condition $v \ln 2 > 1/2$ is satisfied, the CDW phase emerges in the strong-coupling regime. This allows us to infer the existence of a tri-critical point, where Luttinger liquid, CDW insulator and Mott-Hubbard insulator co-exist. Strong-coupling theory to first order indicates that the tri-critical point lies on the line $v_{\text{tp}}^{\text{LR}} = 1/(2 \ln 2)$, i.e., $V \approx 0.72134U$. For the extended $1/r$ -Hubbard model, the same considerations give $v_{\text{tp}}^{\text{NN}} = 1/2$.

The comparison between the $1/r$ -Hubbard models with $1/r$ -long-range and nearest-neighbor interactions shows that the ground-state energy density remains similar for small interaction strengths. Discernible deviations emerge at moderate values of v , e.g., for $v=0.5$, and discrepancies become clearly visible for $v \gtrsim 0.6$. This behavior arises from the fact that the tri-critical point is

reached for smaller v in the case of nearest-neighbor interactions, $v_{\text{tp}}^{\text{NN}} < v_{\text{tp}}^{\text{LR}}$. In comparison with the extended $1/r$ -Hubbard model, the CDW phase requires larger v for $1/r$ -long-range interactions.

B. Two-particle gap

For $V=0$ the two-particle gap is known for all system sizes [6, 20, 22],

$$\Delta_2(L; U \geq 1, V=0) = U - 1 + \frac{2}{L} + \sqrt{(U-1)^2 + \frac{4U}{L}}. \quad (36)$$

In the thermodynamic limit, we find

$$\Delta_2(U \geq 1, V=0) = 2(U-1). \quad (37)$$

The gap opens linearly above the critical interaction strength, $U_c(V=0) = 1$. Eq. (36) shows that the finite-size data approach the value in the thermodynamic limit

$$\Delta_2(L; U, V) = \Delta_2(U, V) + a_2(U, V) \left(\frac{1}{L}\right)^{\gamma_2(U, V)} \quad (38)$$

with $\gamma_2(U \neq U_c, V=0) = 1$, $\gamma_2(U = U_c, V=0) = 1/2$.

More generally, we assume for all (U, V)

$$\gamma_2(U, V) = \begin{cases} 1 & \text{for } U \neq U_c(V) \\ \frac{1}{2} & \text{for } U = U_c(V) \end{cases}. \quad (39)$$

As for the ground-state energy, these exponents apply for very large system sizes. We shall discuss the finite-size modifications in more detail in Sec. IV.

In Fig. 5 we show the DMRG results for $\Delta_2(L; U, V)$ as a function of $1/L$ for various values for U as a function of $1/L$ for $L = 8, 16, 24, 32, 48, 64$ for (a) $v=0.1$, (b) $v=0.3$, (c) $v=0.5$. The lines are fits to the algebraic function in Eq. (38). The fits in Fig. 5 are seen to agree very well with the data, showing a steep decrease of the finite-size gap as a function of inverse system size. This indicates that large system sizes are required to obtain reasonable gap extrapolations.

The extrapolated gaps $\Delta_2(U, V)$ are shown in Fig. 6 as a function of U for $v=0$, $v=0.1$, $v=0.3$, $v=0.4$ and $v=0.5$ for the $1/r$ -Hubbard model with $1/r$ -long-range interactions (crosses) and for the $1/r$ -Hubbard model with nearest-neighbor interactions (open triangles). Finite-size effects smoothen the phase transition which makes it difficult to extract the critical point and the critical exponent for the opening of the Mott-Hubbard gap.

In the bare $1/r$ -Hubbard model, the Mott transition is solely governed by the on-site interaction. Once the Hubbard interaction exceeds the bandwidth, $U > W$, electrons become ‘localized’, and the metallic state goes over to a Mott insulator. In the presence of inter-site interactions, the Mott transition is shifted to larger values which implies a more stable metallic Luttinger liquid.

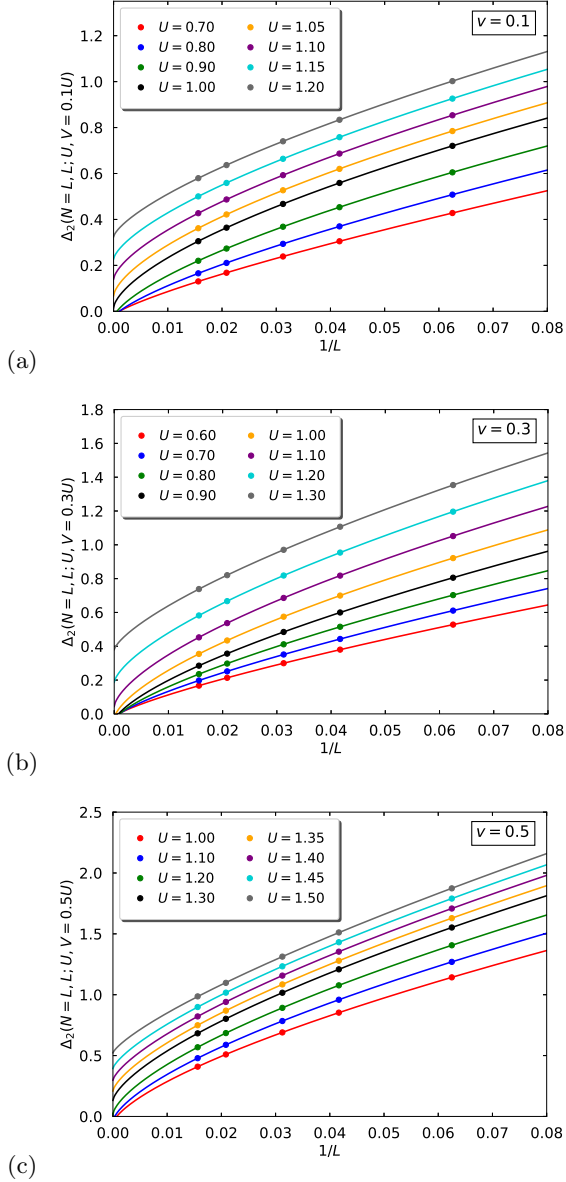


Figure 5. Two-particle gap $\Delta_2(L; U, V)$ for the extended $1/r$ -Hubbard model with $1/r$ -long-range interactions as a function of inverse system size for $L = 8, 16, 24, 32, 48, 64$ and various values for U for (a) $v = 0.1$, (b) $v = 0.3$, (c) $v = 0.5$. The continuous lines are fits to the algebraic fit function (38). The intercept of the extrapolation curves with the ordinate defines the extrapolation estimate $\Delta_2(U, V)$ for the two-particle gap.

At first glance, the shift of the Mott transition to higher values in models with repulsive inter-site interactions seems counterintuitive. From a wave-mechanical viewpoint, however, the repulsive interaction between lattice sites softens the two-particle scattering potential. Figuratively speaking, particles scattered by the weaker interaction V do not fully experience the stronger on-site interaction U . This ties in with the observation that the gap in the $1/r$ -Hubbard model with $1/r$ -long-range

interactions is smaller than that for the extended $1/r$ -Hubbard model for the same v because the long-range parts of the inter-site interaction further smoothen the two-particle scattering potential in position space.

C. Momentum distribution

In Fig. 7 we show the momentum distribution from DMRG at half band-filling for $L = 64$ sites for various values of U and $v = 0.3, v = 0.5$, and $v = 0.7$ (from top to bottom). The momentum distributions resemble those obtained for the extended $1/r$ -Hubbard model. For small interactions, the momentum distribution looks like that of a Fermi liquid with all states $-\pi < k < 0$ occupied and all states $0 < k < \pi$ empty. For small U , low-energy scattering processes are limited to the vicinity of the sole Fermi point $k_F = 0$. Indeed, in the field-theoretical limit, $U, V \ll 1$, the model reduces to a bare g_4 -model of only right-moving particles [17]. This ‘non-interacting Luttinger liquid’ displays a jump discontinuity at k_F .

However, the $1/r$ -Hubbard model is defined on a lattice and the bandwidth is finite. Consequently, there is a left Fermi point at $k_{F,2} = -\pi$ at the lower Brillouin zone boundary where the bare dispersion relation jumps by W . The left Fermi point starts to play a role when U becomes of the order of half the bandwidth. States near $k_{F,2}$ are depleted more quickly as a function of U than those deeper in the Brillouin zone. Therefore, as seen in Fig. 7, the momentum distribution develops a maximum (minimum) around $k = -\pi/2$ ($k = \pi/2$).

These considerations show that the Luttinger param-

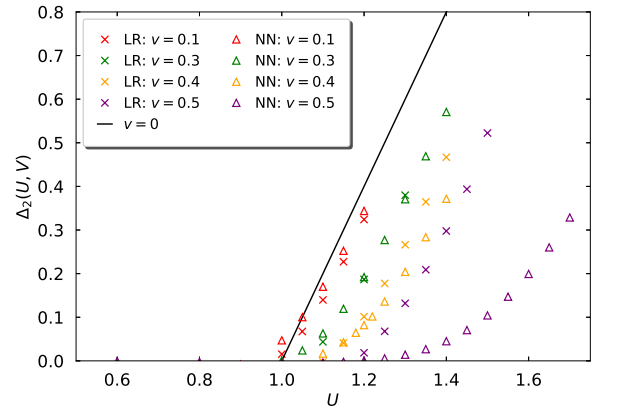


Figure 6. Two-particle gap $\Delta_2(U, V)$ for the $1/r$ -Hubbard model as a function of U for $v = V/U = 0.1$ (red), $v = 0.3$ (green), $v = 0.4$ (orange), $v = 0.5$ (purple), extrapolated from finite-size data with up to $L = 64$ sites. The crosses represent the model with $1/r$ -long-range interactions, the open triangles correspond to the model with only nearest-neighbor interactions [23]. The continuous line is the exact result in the thermodynamic limit for $V = 0$, $\Delta_2(U, V = 0) = 2(U - 1)$, see Eq. (37).

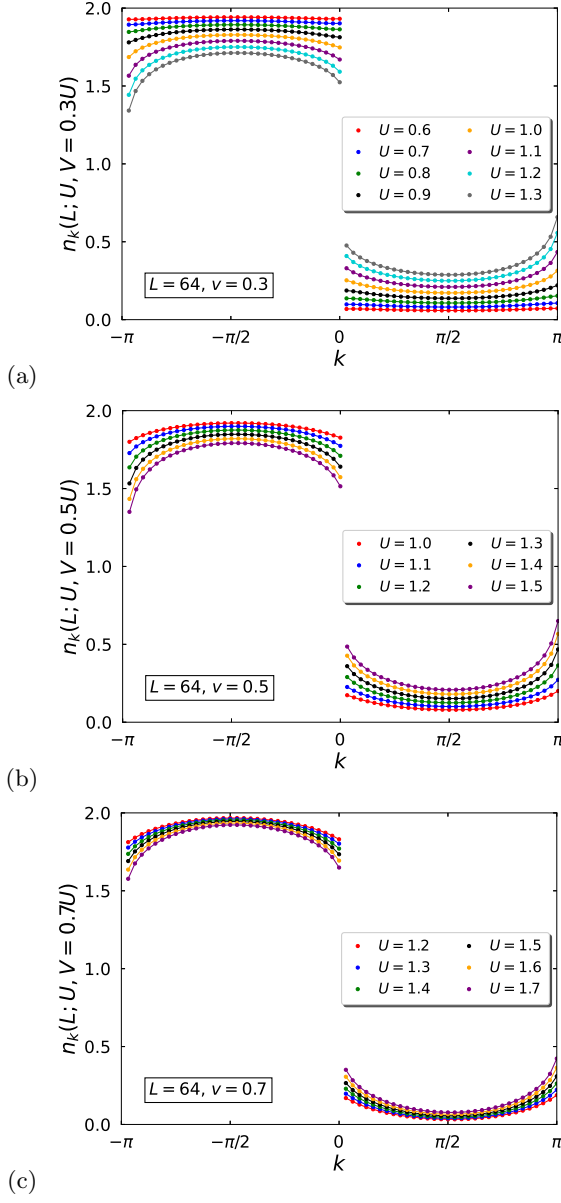


Figure 7. Momentum distribution $n_k(L; U, V)$ at half band-filling for the extended $1/r$ -Hubbard model with $1/r$ -long-range interactions for $L = 64$ sites and for various values for U for $v = 0.3$, $v = 0.5$, and $v = 0.7$ (from top to bottom). Continuous lines are a guide to the eye only.

eter must deviate from unity, $K(U, V) < 1$, for all (U, V) , even though corrections to unity are (exponentially) small for $U, V \ll 1$. Therefore, $n(k)$ is a continuous function in the $1/r$ -Hubbard model for all $U, V > 0$.

D. Structure factor and CDW order parameter

Lastly, we show the structure factor from DMRG in Fig. 8 for $v = 0.3$, $v = 0.5$, and $v = 0.7$ (from top to bottom) for the extended $1/r$ -Hubbard model with $1/r$ -

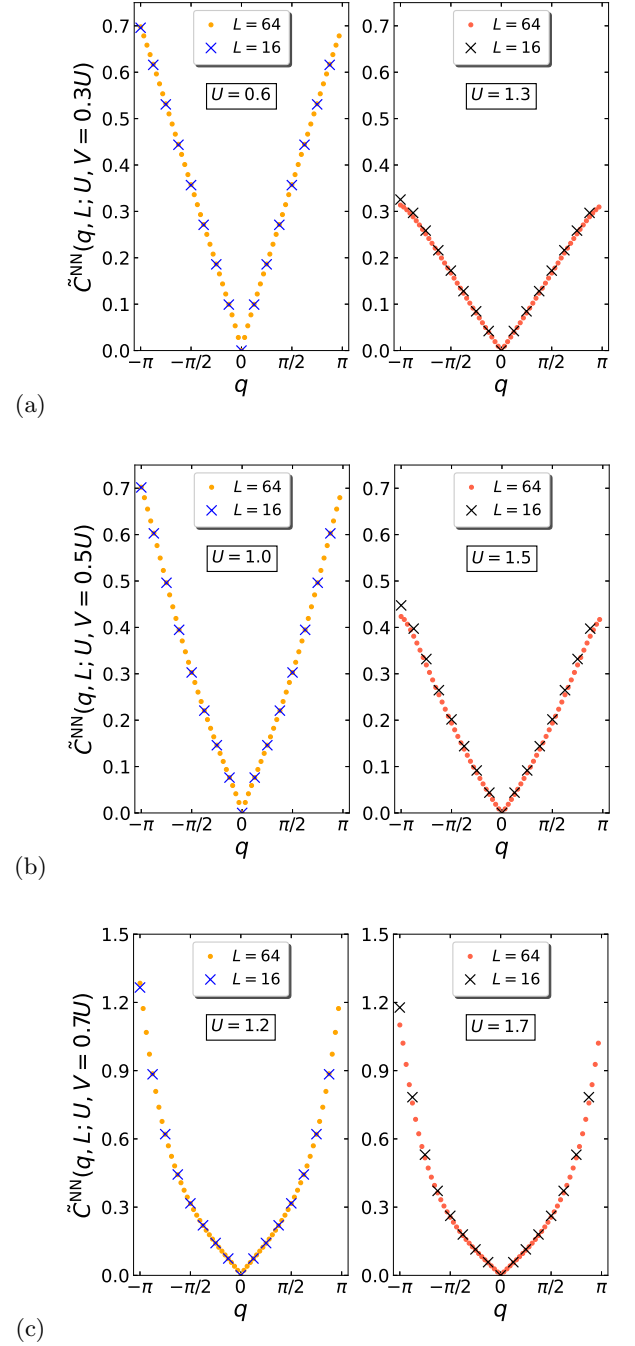


Figure 8. Structure factor $\tilde{C}^{NN}(q, L; U, V)$ for the extended $1/r$ -Hubbard model with long-range interactions for $L = 16, 64$ below (left) and above (right) the Mott transition for (a) $v = 0.3$, (b) $v = 0.5$, (c) $v = 0.7$. Dotted lines are a guide to the eye only.

long-range interactions at system sizes $L = 16, 64$ below (left) and above (right) the Mott transition. As for the momentum distribution, the $1/r$ -Hubbard model with nearest-neighbor interactions and with $1/r$ -long-range interactions lead to the same qualitative behavior.

In general, finite-size effects are fairly small but larger

systems permit a much better resolution in momentum space. In comparison with the exact result for the non-interacting system,

$$\tilde{C}^{\text{NN}}(q, n = 1; U = 0, V = 0) = \frac{|q|}{\pi}, \quad (40)$$

we see that the Hubbard interaction reduces the charge fluctuations. This is expected because the suppression of double occupancies likewise reduces the number of holes and the charges are more homogeneously distributed in the system. Therefore, the charge correlations become smaller when we compare the left and right figure in the same row.

The repulsive inter-site interactions counter the effect of the Hubbard interaction because pairs of a double occupancy and a hole are energetically favorable. Therefore, the charge correlations increase when we go from top to bottom in the left/right row, even though U also increases from top to bottom.

When the interactions between the electrons on different lattice sites increase beyond a certain threshold value $V_c^{\text{CDW}}(U)$, the ground state displays charge-density-wave order. In Fig. 9a we show the charge-density-wave order parameter $N_\pi(L; U = 1.3, V)$, see Eq. (28), as a function of $1/L$ for various values of V , and the extrapolated result $N_\pi(U = 1.3, V)$ into the thermodynamic limit using a second-order polynomial fit in Fig. 9b,

$$N_\pi(L; U, V) = N_\pi(U, V) + \frac{N_1(U, V)}{L} + \frac{N_2(U, V)}{L^2}. \quad (41)$$

Apparently, the CDW order parameter is continuous over the CDW transition. Close to the transition, $V \gtrsim V_c(U)$,

$$N_\pi(U, V) = N_0 [V - V_c(U)]^{2\nu}, \quad (42)$$

where ν is the critical exponent for the CDW order parameter $D(U, V)$. Note that, in our previous article on the extended $1/r$ -Hubbard model [23], we used data for $\nu = 0.7$ to compute the order parameter. Here, we trace the CDW transition as a function of V for fixed U .

To make use of Eq. (42), the critical interaction $V_c(U)$ must be known. In addition, the region of validity of Eq. (42) is unknown *a priori*. Typically, one has to study system parameters close to the transition to obtain a reliable estimate for ν . Therefore, very large system sizes might be necessary to reach the scaling limit, and we have to be satisfied with the result from Fig. 9b that the CDW transition at $U = 1.3$ is continuous with exponent $\nu \leq 1/2$.

IV. MOTT TRANSITIONS

In this section, we determine the critical value for the Mott-Hubbard and CDW transitions in the $1/r$ -Hubbard model with $1/r$ -long-range interactions. We investigate the two-particle gap, the ground-state energy, the Luttinger parameter, and the structure factor at the Brillouin zone boundary to locate the critical interaction strengths $U_c^{\text{Mott}}(V)$ and $U_c^{\text{CDW}}(V)$.

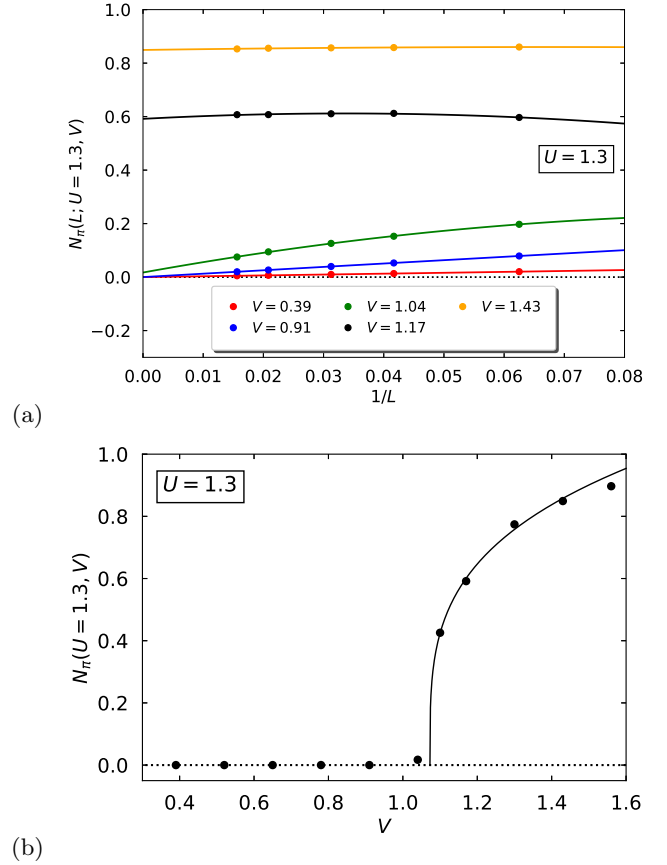


Figure 9. (a) CDW order parameter $N_\pi(L; U = 1.3, V)$ for the half-filled $1/r$ -Hubbard model with $1/r$ -long-range interactions as a function of $1/L$ ($L \leq 64$) for fixed $U = 1.3$ and various V -values. Lines are a second-order polynomial fit in $1/L$, see Eq. (41); (b) Extrapolated CDW order parameter $N_\pi(U = 1.3, V)$ as a function of V . The line is an algebraic fit to the data in the vicinity of the CDW transition, see Eq. (42), with $V_c(U = 1.3) = 1.07$, $N_0 = 1.14$ and $2\nu = 0.27$.

A. Two-particle gap

To simplify the notation, we drop the superscript ‘Mott’ when quantities cannot be confused with those for the CDW transition.

In our previous work [22], we showed that the exponent $\gamma_2(U) = \gamma_2(U, V = 0)$ sensitively depends on U in the vicinity of the Mott-Hubbard transition, and the critical interaction for the bare $1/r$ -Hubbard model, $U_c(V = 0) = 1$, was obtained with an accuracy of one per mil. Moreover, we demonstrated in section IV A of [23] that the minimum of the γ -parameter depends only marginally on the system size, especially for $L \geq 16$.

In Fig. 10 we display the exponent $\gamma_2(U, V)$, as obtained from the fit of the finite-size data in the range $16 \leq L \leq 64$ to the algebraic function in Eq. (38). Also shown are the quartic fits around the minima which lead to the critical interactions $U_{c,\text{gap}}(V)$, listed below in Ta-

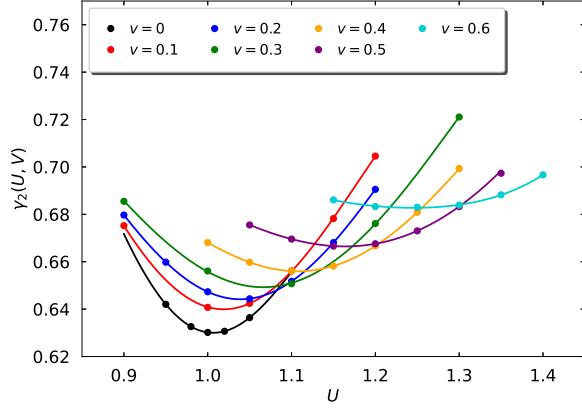


Figure 10. Exponent $\gamma_2(U, V)$ for the two-particle gap in the extended $1/r$ -Hubbard model with $1/r$ -long-range interactions as a function of U for various values of $v = V/U$, based on system sizes $16 \leq L \leq 64$. The minimum of the curve determines $U_{c,\text{gap}}(V)$.

ble I. Note that the curves flatten out for increasing v . Therefore, it is not possible to determine quantum-phase transitions for $v \gtrsim 0.7$ from the parameter $\gamma_2(U, V)$ for system sizes $L \leq 64$ and step size $\Delta U = 0.05$.

The comparison with the exact value for $V = 0$ shows that the gap exponent $\gamma_2(U, V)$ provides a fairly accurate estimate for the critical interaction. The same accuracy can be obtained when using the ground-state energy exponent $\gamma_0(U, V)$, as we shall show next.

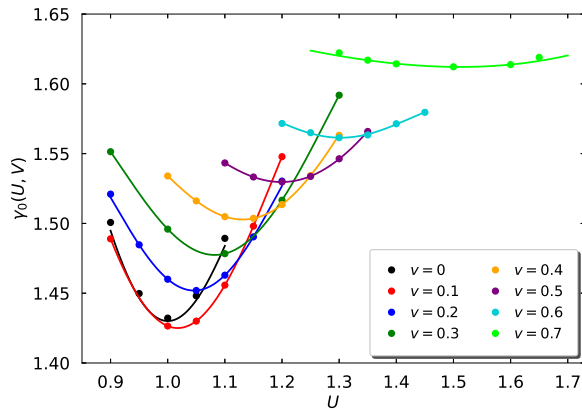


Figure 11. Exponent $\gamma_0(U, V)$ for the ground-state energy of the extended $1/r$ -Hubbard model with $1/r$ -long-range interactions as a function of U for various values of $v = V/U$, based on system sizes $16 \leq L \leq 64$. The minimum of the curve determines $U_{c,\text{gs}}(V)$.

V/U	$U_{c,\text{gap}}(V)$	$U_{c,\text{gs}}(V)$	$U_{c,\text{LL}}(V)$	$U_{c,\text{sf}}(V)$	$\overline{U}_c(V)$
0	1.009	1.000	1.033	0.965	1.002
0.1	1.019	1.017	1.058	0.979	1.018
0.2	1.039	1.046	1.089	0.999	1.043
0.3	1.066	1.082	1.129	1.031	1.077
0.4	1.108	1.131	1.183	1.071	1.123
0.5	1.164	1.199	1.261	1.132	1.189
0.6	1.245	1.303	1.388	1.232	1.292
0.7	—	1.512	1.684	1.404	1.533

Table I. Critical interaction strengths for the extended $1/r$ -Hubbard model with $1/r$ -long-range interactions, as obtained from the two-particle gap, the ground-state energy, the Luttinger parameter, and the structure factor for systems with $16 \leq L \leq 64$ lattice sites. For $V = 0$, the exact result in the thermodynamic limit is known [20], $U_c(V = 0) = 1$.

B. Ground-state energy

As seen from Eq. (35), the $1/L$ corrections to the ground-state energy density also permit to locate the Mott transition in the extended $1/r$ -Hubbard model, in the same way as the two-particle gap. In Fig. 11 we show the exponent $\gamma_0(U, V)$, as obtained from the fit of the finite-size data in the range $16 \leq L \leq 64$ to the algebraic function in Eq. (34). Also shown in the figure are the quartic fits around the minima which lead to the critical interactions $U_{c,\text{gs}}(V)$ listed in Table I.

As seen from Table I, the critical interaction strengths obtained from the minima of $\gamma_0(U, V)$ very well agree with the exact result at $V = 0$ and also with the values obtained from the gap exponent $\gamma_2(U, V)$, with deviations in the low percentage range. Therefore, we find reliable estimates for the critical interaction strength for the Mott transition from $\gamma_0(U, V)$ and $\gamma_2(U, V)$.

C. Luttinger parameter

As an alternative to locate the Mott transition, we monitor the Luttinger parameter and, for fixed ratios $v = V/U$ [22], we determine $U_c(U, V)$ from the condition [17]

$$K(U_c(V), v) = 1/2. \quad (43)$$

As an example, in Fig. 12 we show the Luttinger parameter $K(L; U, V)$ from DMRG for the $1/r$ -Hubbard model with $1/r$ -long-range interaction $V = 0.3U$ as a function of U for system sizes $L = 8, 16, 24, 32, 48, 64$ including a second-order polynomial extrapolation to the thermodynamic limit. The intersection of the extrapolation into the thermodynamic limit with $K_c = 1/2$ determines $U_c(V)$.

To obtain a reliable estimate for the intersection we can either use the two data points closest to the transition and perform a linear interpolation, in this case from $U = 1.1$ and $U = 1.2$. Alternatively, we use a

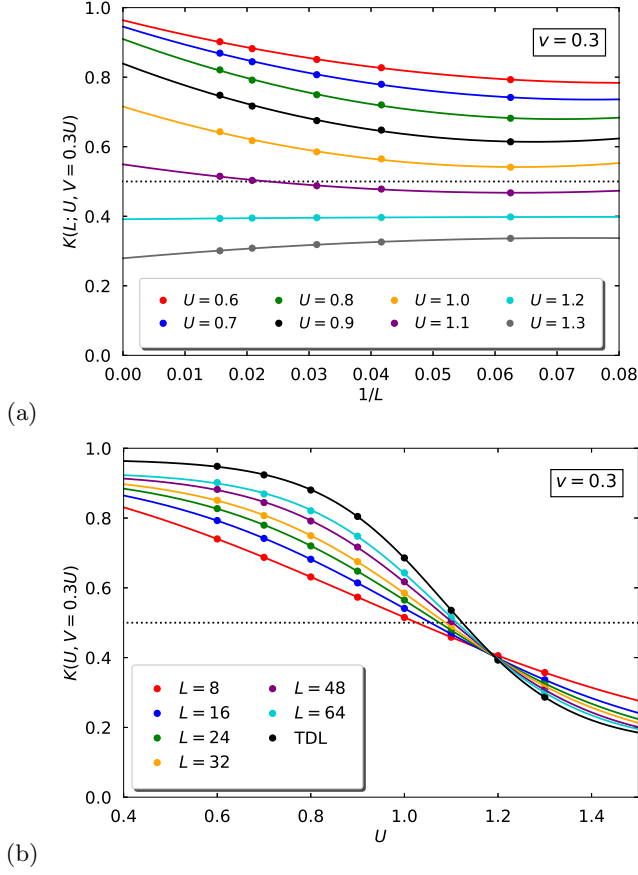


Figure 12. Luttinger parameter $K(L; U, V)$ from DMRG for the $1/r$ -Hubbard model with $1/r$ -long-range interactions for $v = 0.3$. (a) K as a function of inverse system size for $L = 16, 24, 32, 48, 64$ for various values for U including a second order polynomial fit to the thermodynamic limit. (b) K as a function of U for system sizes $L = 8, 16, 24, 32, 48, 64$. The lines correspond to the fit from Eq. (44). The intersection of the extrapolation with $K_c = 1/2$ determines $U_{c,LL}(V)$. The black line represents the thermodynamic limit (TDL), obtained from the fits in Fig. 12a.

four-parameter fit of the whole data set that employs the information that the Luttinger parameter deviates from unity by exponentially small terms for $U, V \rightarrow 0$,

$$K(U, V) = a + b \tanh(c + dU) \quad (44)$$

to fit the extrapolated data for finite values of U to a continuous curve which is parameterized by a, b, c, d that depends on v . Then, we solve Eq. (43) for $U_{c,LL}(V)$.

Alternatively, we could have solved Eq. (43) for each system size, and extrapolated the resulting system-size dependent critical interactions strengths to the thermodynamic limit. Since the results deviate more strongly from the exact value for $V = 0$, we refrain from pursuing this approach further.

As seen from Table I, the critical value from the Luttinger parameter systematically overestimates the correct interaction strengths by some five percent. The

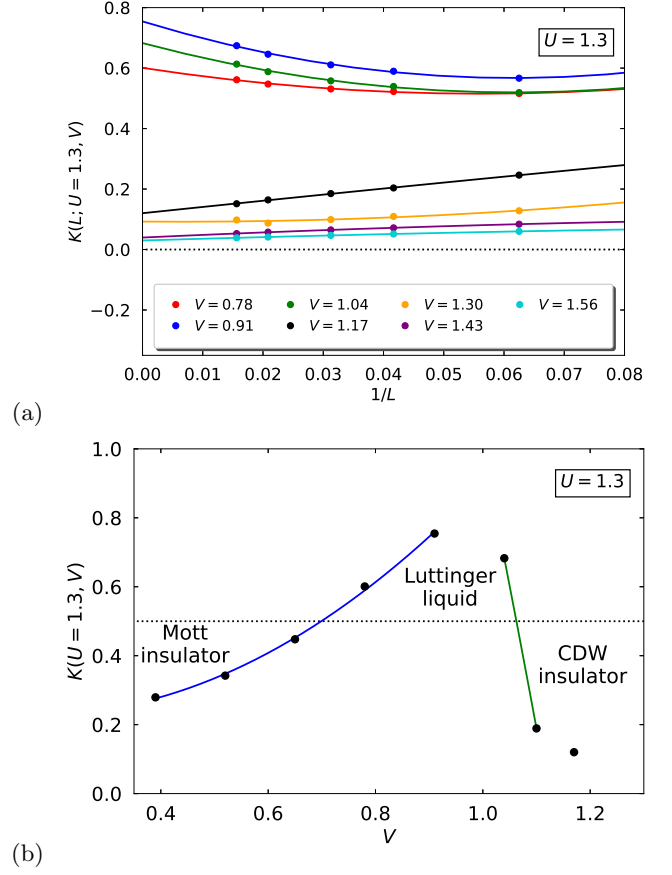


Figure 13. Luttinger parameter $K(L; U, V)$ from DMRG for the $1/r$ -Hubbard model with $1/r$ -long-range interactions for fixed $U = 1.3$; (a) as a function of inverse system size for $L = 16, 24, 32, 48, 64$ for various values for V including a second order polynomial fit to the thermodynamic limit. (b) as a function of V in the thermodynamic limit. The lines correspond to a first-order (green) and second-order (blue) polynomial fit.

same overshooting was found for the CDW transition in a one-dimensional model for spinless fermions with nearest-neighbor interactions [26].

Apparently, much larger systems are required to overcome this systematic error. As in Ref. [23], we use the critical interaction strengths $U_{c,LL}(V)$ as an upper bound to the exact value $U_c(V)$.

D. Transitions at fixed Hubbard interaction

Since the Luttinger parameter characterizes electron correlations and explicitly identifies the Luttinger liquid, this parameter allows for the identification of two quantum phase transitions within a single plot, as we observe only the breakdown of the Luttinger liquid, see Fig. 13. The system enters a Luttinger liquid phase once the Luttinger parameter exceeds $K > 1/2$.

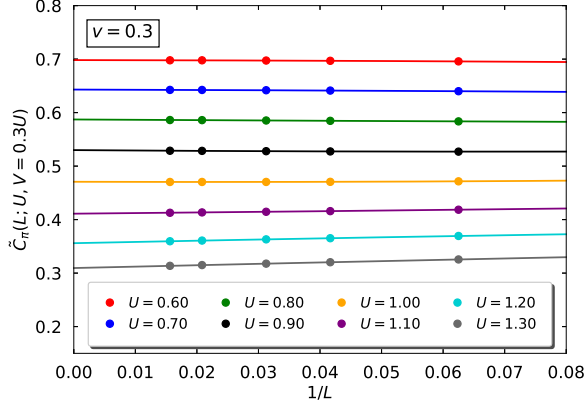


Figure 14. Structure factor $\tilde{C}^{\text{NN}}(\pi, L; U, V)$ as a function of $1/L$ for various values of U for the $1/r$ -Hubbard model with $1/r$ -long-range interaction $v = 0.3$ for system sizes $L = 16, 24, 32, 48, 64$. Lines are a second-order polynomial extrapolation to the thermodynamic limit, see Eq. (45).

However, achieving the theoretical value of $K = 1$ within the metallic Luttinger liquid is hindered by finite-size effects. Note that the results from Fig. 13 lead to the vertical lines for $U = 1.3$ in the phase diagram.

Of course, it is not possible to specify the nature of the insulating phases from the Luttinger parameter alone. One might argue that, due to finite-size effects, the phase transition into the CDW phase is more easily detected, i.e., the curve $K(U, V)$ for fixed U is steeper as a function of V in the CDW phase than in the Mott insulating phase.

This ambiguity does not pose a problem because other physical quantities, e.g., the structure factor, permit to identify the CDW phase, as we discuss next.

E. Structure factor

For the $1/r$ -Hubbard model, the finite-size corrections to the structure factor $\tilde{C}_\pi(L; U, V) \equiv \tilde{C}^{\text{NN}}(\pi, L; U, V)$,

$$\tilde{C}_\pi(L; U, V) = \tilde{C}_\pi(U, V) + \frac{C_1(U, V)}{L} + \frac{C_2(U, V)}{L^2}, \quad (45)$$

permit to locate the critical interaction strength. In Fig. 14 we show the structure factor for $v = 0.3$ and various values of U as a function of inverse system size for $L = 16, 24, 32, 48, 64$.

As can be seen from the figure, the coefficient in $1/L$ changes its sign at the critical interaction strength,

$$C_1(U_{\text{c, sf}}^{\text{Mott}}(V), V) = 0. \quad (46)$$

To see this more clearly, in Fig. 15 we show the coefficient $C_1(U, V)$ as a function of U for $v = 0.1, v = 0.3, v = 0.5$,

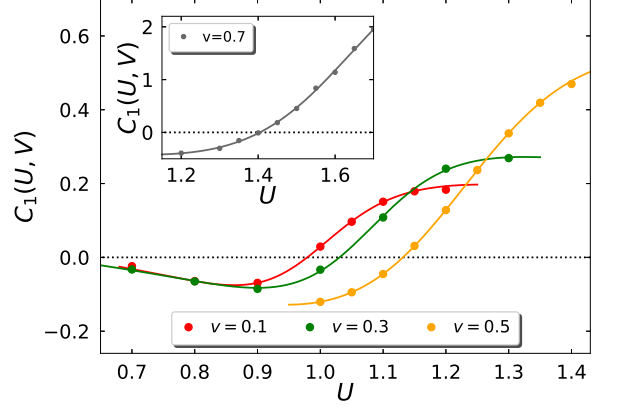


Figure 15. Finite-size coefficient $C_1(U, V)$ of the structure factor as a function of U for the $1/r$ -Hubbard model with $1/r$ -long-range interactions for $v = 0.1, v = 0.3$, and $v = 0.5$ (inset: $v = 0.7$), see Eqs. (45) and (46). Lines are fitted Fano resonance curves (47).

and $v = 0.7$ and fit the data to a Fano resonance,

$$C_1^{\text{Fano}}(U, V) = a(V) + b(V) \frac{[q_F(V)\Gamma(V) + U - U_c(V)]^2}{[\Gamma(V)]^2 + [U - U_c(V)]^2}. \quad (47)$$

Analogously, we find the critical interaction strength $U_c^{\text{CDW}}(V)$ for the transition into the CDW phase from the $1/L$ corrections to the CDW order parameter (28), $N_1(U, V)$ in Eq. (41), instead of $C_1(U, V)$.

As in our two previous studies of the $1/r$ -Hubbard model [22, 23], a bound state that interacts with the continuum manifests in observables, thereby contributing a Fano resonance to various physical quantities, with weight of the order $1/L$. Using the Fano resonance formula and the conditions $C_1(U_{\text{c, sf}}^{\text{Mott}}, V) = 0$ and $N_1(U_{\text{c, sf}}^{\text{CDW}}, V) = 0$, respectively, the $1/L$ -corrections of the structure factor and of the CDW order parameter provide the estimate $U_{\text{c, sf}}(V)$ for the critical interaction. The resulting data for various v are listed in Table I.

The critical interaction strength $U_{\text{c, sf}}^{\text{Mott}}(V)$ systematically underestimates the exact value for the Mott transition by a few percent. Together with the critical interaction strength from the Luttinger parameter $U_{\text{c, LL}}^{\text{Mott}}(V)$ we thus can set tight limits to $U_c^{\text{Mott}}(V)$.

F. Identification of the CDW

Lastly, we discuss the phase transitions between the metallic Luttinger liquid and the charge-density wave insulator. For this case, the γ -parameters of the ground-state energy, γ_0 , and of the two-particle gap, γ_2 , are no longer suitable. Instead, we address the Luttinger parameter and the order parameter of the charge-density wave. We qualitatively assess the CDW transition by

observing the opening of the two-particle gap, as shown in Fig. 6. A quantitative analysis would require much larger system sizes and a wider range of data points to reduce finite-size effects. We solely use the two-particle gap to verify the consistency of our results.

1. Luttinger parameter and CDW order parameter

As shown in Fig. 13, the Luttinger parameter serves as an indicator for the CDW phase transition. The missing logarithmic corrections induce an inaccuracy in the quantitative determination of the critical interaction. In any case, the Luttinger parameter permits to identify easily phase transitions to/from a Luttinger liquid phase.

To estimate the error in the Luttinger parameter for curves with fixed U , the Mott transition on the left side of Fig. 13b can be used as a reference. While the depicted phase transition is determined at $V_{c,LL}^{\text{Mott}}(U = 1.3) \approx 0.699$, the fit of all Mott transitions from Section V A 2 gives a critical interaction $V_c^{\text{Mott}}(U = 1.3) \approx 0.773$, corresponding to a deviation of approximately 10%.

The CDW order parameter can be evaluated as shown in Fig. 9. Due to finite-size effects, the phase transition appears to be continuous, requiring a large number of data points beyond the transition for an accurate quantitative determination.

2. Fano resonance curve

As demonstrated in our previous works [22, 23] and in Section IV E, a bound state exists that couples to the continuum, thereby inducing Fano resonances in various physical quantities. This behavior is also seen in the parameter $N_1(U, V)$ within the order parameter of the CDW, as defined in Eq. (41); see, e.g., Fig. 14b in [23]. The phase transition can be clearly identified through the sign change of the parameter $N_1(U, V)$, see Fig. 16 for fixed $U = 0.2$ and $U = 1.3$ in the inset.

Due to the limited number of data points, particularly after the sign change, a full verification of the Fano resonance curve (47) is not possible. However, the available data points align well with the fitted curve. Moreover, once two data points are available, situated just before and after the transition, a simple linear fit function is sufficient to provide reasonable estimates for the transition.

In Table II we collect the results for the CDW transitions at fixed $U = 0.2, 1.3$ and for $v = V/U = 1$. It is seen that the estimate from the extrapolation of the order parameter in Fig. 9, $V_{c,op}(U = 1.3) = 1.07$, is in good agreement with the result from the Luttinger and Fano extrapolations, $\bar{V}_c(U = 1.3) = 1.076$, as collected in Table II.

All approaches lead to consistent results. The extrapolations from the Luttinger parameter underestimate the critical interactions whereas the results from the Fano resonance give an upper bound to $V_c^{\text{CDW}}(U)$. As for the

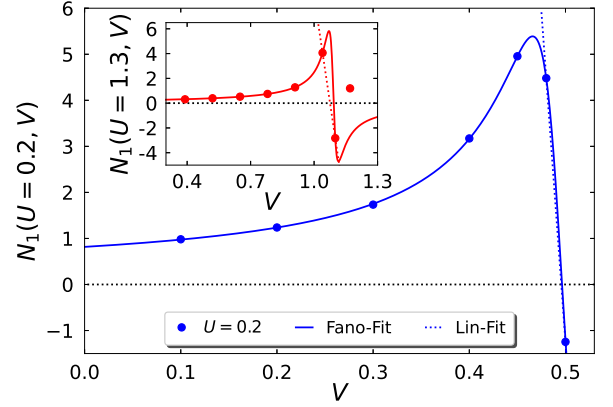


Figure 16. $N_1(U, V)$ as a function of V and fixed U for the extended $1/r$ -Hubbard model with $1/r$ -long-range interactions for $U = 0.2$ (inset: $U = 1.3$). Lines are fitted Fano resonance curves (47) and dotted lines are linear fits. To stabilize the fit for $U = 1.3$, we did not include the data point for $V = 1.17$.

U	$V_{c,LL}(U)$	$V_{c,N_1}^{\text{Fano}}(U)$	$V_{c,N_1}^{\text{Lin}}(U)$	$\bar{V}_c^{\text{CDW}}(U)$
0.2	0.493	0.496	0.496	0.495
1.3	1.062	1.093	1.075	1.076

$v = V/U$	$U_{c,LL}(V)$	$U_{c,N_1}^{\text{Fano}}(V)$	$U_{c,N_1}^{\text{Lin}}(V)$	$\bar{U}_c^{\text{CDW}}(V)$
1.0	0.762	0.800	0.783	0.782

Table II. Critical interaction strengths for the metal-to-CDW insulator transition in the $1/r$ -Hubbard model with $1/r$ -long-range interactions, as obtained from the Luttinger parameter $V_{c,LL}$ and the parameter $N_1(U, V)$ from Eq. (41) using a Fano resonance fit function $V_{c,N_1}^{\text{Fano}}(U)$, see Eq. (47), or a linear fit function $V_{c,N_1}^{\text{Lin}}(U)$; in DMRG, $16 \leq L \leq 64$ lattice sites were addressed.

Mott transition, this permits to set boundaries to the exact critical value of the metal-to-insulator transition.

V. RENORMALIZATION OF THE PHASE DIAGRAM

In this section, we discuss the quantum phase diagram for the $1/r$ -Hubbard model with $1/r$ -long-range interactions and its mapping from the quantum phase diagram of the $1/r$ -Hubbard model with nearest-neighbor interactions.

A. Quantum phase diagrams

For convenience, we reproduce the quantum phase diagrams in Fig. 1 in Fig. 17, where we add the Hartree-Fock results for the transition between metal and CDW insu-

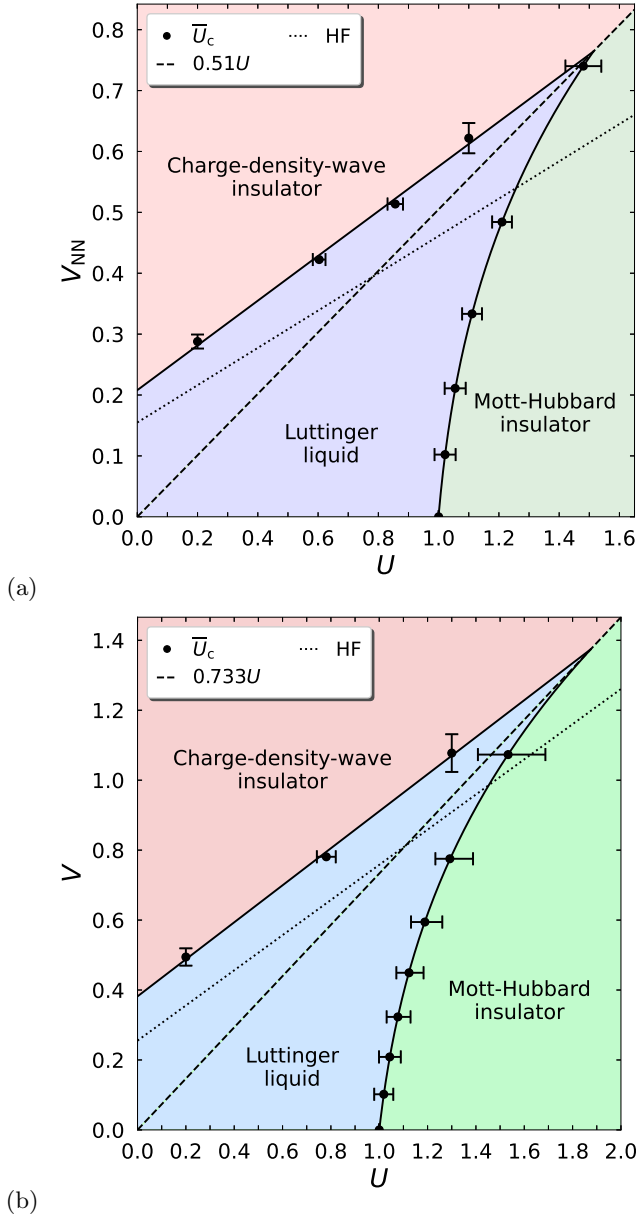


Figure 17. (a) Phase diagram of the one-dimensional $1/r$ -Hubbard model with nearest-neighbor interactions. (b) Phase diagram of the one-dimensional $1/r$ -Hubbard model with $1/r$ -long-range interactions. Continuous lines: polynomial fits of the phase-separation lines, see Sects. VA 1 and VA 2; dotted line: Hartree-Fock (HF) result for the transition between metal and charge-density-wave insulator.

lator as dotted lines and the strong-coupling limit for the separation lines between Mott-Hubbard and CDW insulators as dashed lines, respectively. As in our previous work [23], we refrain from the analysis of the transition between Mott and CDW insulators.

As shown numerically for the standard extended Hubbard model [32–35], the transition is discontinuous for large interactions, $U, V \gg W$, as also inferred from the

atomic limit, see appendix, where $V_{NN,c}^{\text{al}} = U/2$ for the extended Hubbard model. Since the kinetic energy slightly stabilizes the Mott-Hubbard insulator, the phase separation line in Fig. 17a for large interactions is approximately given by $V_{c,NN}(U \gg W) \approx 0.51U$ (dashed line). The same line of reasoning gives $V_{c,LR}^{\text{al}} = U/[2\ln(2)]$ in the atomic limit in the presence of $1/r$ -long-range interactions, and $V_{c,LR}(U \gg W) \approx 0.733U \approx 0.51U/\ln(2)$ (dashed line).

For the standard extended Hubbard model and for moderate interactions, $U, V \approx W$, and fixed U , a transition occurs from the Mott insulator to a bond-order-wave insulator as a function of V before the CDW insulator dominates at large nearest-neighbor interactions. Beyond the triple point where Luttinger liquid, Mott insulator, and CDW insulator meet in our phase diagrams, we also expect to find a region with a bond-order wave in extended $1/r$ -Hubbard models. Therefore, the dashed line separating Mott-Hubbard insulator and charge-density-wave insulator should be taken as a guide to the eye only. For this reason, we only show the phase diagram for $U \leq 1.9$, and the analysis of the triple point and the bond-order wave phase are beyond the scope of our present work.

1. Parameterization of the CDW critical line

For $U \leq 1.9$, the transition from the Luttinger liquid to the CDW insulator is qualitatively correctly described by Hartree-Fock theory. In very good approximation, the critical interactions $V_c^{\text{CDW}}(U)$ are linear functions of U . As shown in the appendix, the dotted Hartree-Fock lines in Fig. 17 are given by

$$V_{c,\text{HF}}^{\text{CDW}}(U) = a^{\text{HF}} + b^{\text{HF}}U + \mathcal{O}(U^2) \quad (48)$$

with

$$\begin{aligned} a_{\text{NN}}^{\text{HF}} &\approx 0.1548 & , & & b_{\text{NN}}^{\text{HF}} &\approx 0.3064, \\ a_{\text{LR}}^{\text{HF}} &\approx 0.2553 & , & & b_{\text{LR}}^{\text{HF}} &\approx 0.5027, \end{aligned} \quad (49)$$

for the $1/r$ -Hubbard models with nearest-neighbor and $1/r$ -long-range interactions, respectively.

Hartree-Fock theory overestimates the stability of the CDW phase and thus underestimates the critical interaction strength, $V_{c,\text{HF}}^{\text{CDW}}(U) < V_c^{\text{CDW}}(U)$. Therefore, in Fig. 17, the dotted Hartree-Fock lines systematically lie below the CDW transition lines derived from our DMRG data, see Table II for the $1/r$ -Hubbard model with $1/r$ -long-range interactions and Table I in our previous work [23] for the $1/r$ -Hubbard model with nearest-neighbor interactions.

For a quantitative comparison, we use the mean values from Table II and apply a linear fit to the three data points to avoid over-fitting and for a direct comparison with the Hartree-Fock results. We thus write

$$V_{c,\text{CDW}}(U) = a^{\text{CDW}} + b^{\text{CDW}}U + \mathcal{O}(U^2), \quad (50)$$

and find

$$\begin{aligned} V_{c,NN}^{\text{CDW}}(U) &\approx 0.2079 + 0.3675U, \\ V_{c,LR}^{\text{CDW}}(U) &\approx 0.3818 + 0.5293U \end{aligned} \quad (51)$$

for the models with nearest-neighbor and $1/r$ -long-range interactions, respectively. Equation (51) defines the continuous phase separation lines between Luttinger liquid and CDW insulator in Fig. 17.

2. Parameterization of the Mott critical line

For purely local interactions, the Mott-Hubbard transition is known to occur at $U_c^{\text{Mott}}(V=0) = 1$ [6, 20], an analytical result that is well reproduced by DMRG [22], see also Table I. The inclusion of repulsive interactions beyond the purely local Hubbard interaction stabilizes the metallic phase, i.e., non-local interactions *increase* the critical interaction strength, $U_c^{\text{Mott}}(V > 0) \geq 1$. Apparently, the additional repulsive interaction softens the two-particle scattering potential in position space and thus makes it less effective.

In the phase diagrams 17 we show $V_c^{\text{Mott}}(U)$ which displays a fairly steep dependence on U close to $U = 1$. In turn, its inverse function, $U_c^{\text{Mott}}(V)$, is a fairly flat function of V around $V = 0$ so that a Taylor series of $U_c^{\text{Mott}}(V)$ in V around the bare Hubbard limit converges much better than a Taylor series of $V_c^{\text{Mott}}(U)$ in U around $U = 1$.

In Fig. 18 we show the data for $U_c^{\text{Mott}}(V)$ for the Mott transition for the $1/r$ -Hubbard models with nearest-neighbor and $1/r$ -long-range interactions, respectively.

For the data points we use the mean values of Table I in this work and in Ref. [23]. For the fit we employ a third-order polynomial,

$$U_c^{\text{Mott}}(V) = b_0 + b_1V + b_2V^2 + b_3V^3, \quad (52)$$

where b_i naturally differ for nearest-neighbor and $1/r$ -long-range interactions. The corresponding critical lines, $V_c^{\text{Mott}}(U)$, are shown in the phase diagrams 17. In the range $1 \leq U \leq 1.9$ and due to the fact that b_3 is small enough, we can approximate

$$V_c^{\text{Mott}}(U) \approx \frac{-b_1 + \sqrt{b_1^2 - 4(b_0 - 1)b_2 + 4b_2(U - 1)}}{2b_2} \quad (53)$$

with very good accuracy. Since $b_0 \approx 1$ and $b_1 \ll 1$, at first glance the critical curve $V_c^{\text{Mott}}(U)$ seems to display a square-root singularity near $U = 1$. However, this is not the case as the critical line does not display any singularities around $(U = 1, V = 0)$.

Nevertheless, the fits for $U_c^{\text{Mott}}(V)$ performed in Fig. 18 deserve special attention. It is important to include at least one data point for attractive interactions, $v = V/U = -0.3$ for nearest-neighbor interactions and $v = -0.2$ for $1/r$ -long-range interactions. Otherwise, the fitted curve would exhibit a nonsensical minimum close to

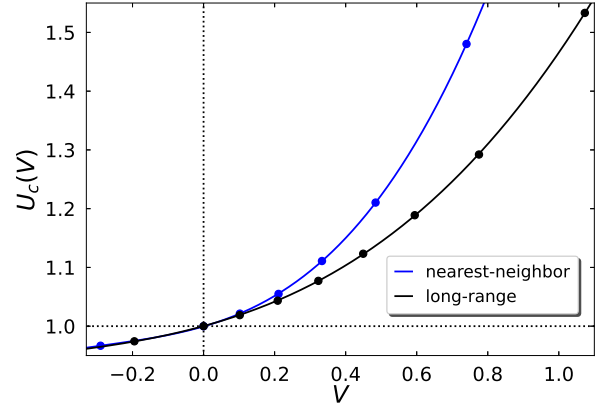


Figure 18. Cubic fits, eq. (52), for the critical interactions $U_c^{\text{Mott}}(V)$ for the Mott transitions in the $1/r$ -Hubbard models with nearest-neighbor interactions (blue solid line) and $1/r$ -long-range interactions (black solid line).

$V = 0$ that would prohibit the inversion of the function. From a physical point of view, an attractive nearest-neighbor interaction de-stabilizes the Luttinger liquid because the Hubbard scattering potential becomes more prominent in position space, jumping from $-|V|$ for electrons on neighboring sites to $+U$ for on-site pairs.

The (stabilized) fit results in the curves

$$\begin{aligned} U_{c,LR}^{\text{Mott}}(V) &= 1.0002 + 0.1659V + 0.1851V^2 + 0.1145V^3, \\ U_{c,NN}^{\text{Mott}}(V) &= 0.9996 + 0.1760V + 0.3362V^2 + 0.4104V^3. \end{aligned} \quad (54)$$

Recall that $U_c^{\text{Mott}}(V=0) = 1$ so that the observation $|b_0 - 1| \ll 1$ implies a very good quality of the fit. The inverse of $U_c^{\text{Mott}}(V)$ is shown in the phase diagram 17.

B. Renormalization

Fig. 17 shows that the two phase diagrams display the same qualitative features. Moreover, as we shall argue now, it is possible to map the two phase diagrams onto each other using simple renormalization factors for the phase transition lines for the CDW and Mott transitions, respectively.

1. CDW transition

As can be seen in Fig. 17 and inferred quantitatively from Eqs. (48)–(51), the phase transition curves between the Luttinger liquid and CDW insulator are very well approximated by straight lines. The corresponding renor-

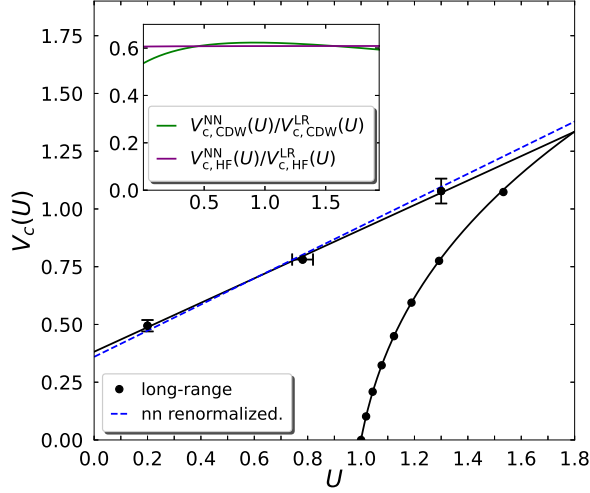


Figure 19. Renormalization of the CDW phase transition line. The phase transitions for the $1/r$ -Hubbard model with $1/r$ -long-range interactions are shown as black dots and lines, together with the renormalized CDW phase transition line from the $1/r$ -Hubbard model with nearest-neighbor interactions (blue dashed line); here, we applied the renormalization factor $R_{\text{CDW}} = 0.61$. The inset displays the exact ratio $V_{\text{c,NN}}^{\text{CDW}}(U)/V_{\text{c,LR}}^{\text{CDW}}(U)$ (green solid line) and Hartree-Fock ratio $V_{\text{c,NN}}^{\text{HF}}(U)/V_{\text{c,LR}}^{\text{HF}}(U)$ (purple solid line) that are close to $R_{\text{CDW}} \approx 0.61$ for all $0 \leq U \leq 1.9$.

malization is given by

$$R_{\text{exact}}^{\text{CDW}}(U) = \frac{V_{\text{c,NN}}^{\text{CDW}}(U)}{V_{\text{c,LR}}^{\text{CDW}}(U)} \quad (55)$$

$$\approx \frac{0.2079 + 0.3675U}{0.3818 + 0.5293U} \approx 0.5445 + 0.2077U.$$

The corresponding result from Hartree-Fock theory is given by

$$R_{\text{HF}}^{\text{CDW}}(U) = \frac{V_{\text{c,NN}}^{\text{HF}}(U)}{V_{\text{c,LR}}^{\text{HF}}(U)} \quad (56)$$

$$\approx \frac{0.1548 + 0.3064U}{0.2553 + 0.5027U} \approx 0.6063 + 0.0062U.$$

Both curves are shown in the inset of Fig. 19. The comparison shows that the factors $R_{\text{exact}}^{\text{CDW}}(U)$ and $R_{\text{HF}}^{\text{CDW}}(U)$ fairly agree with each other over the region of interest, $0 \leq U \leq 1.9$. Recall that the critical interactions from DMRG carry an error estimate.

Since $R_{\text{HF}}^{\text{CDW}}(U)$ is almost independent of U , we choose

$$R_{\text{CDW}} = R_{\text{HF}}^{\text{CDW}}(U=0) \approx 0.61 \quad (57)$$

as our overall renormalization factor for the CDW transition. In Fig. 19 we plot the phase separation lines for the $1/r$ -Hubbard model with $1/r$ -long-range interactions together with the renormalized phase transition line for

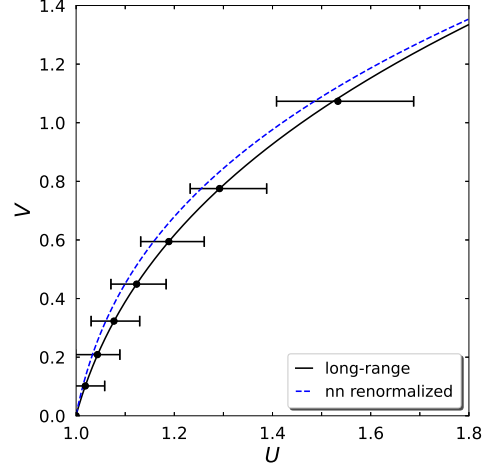


Figure 20. Renormalization of the Mott-Hubbard phase transition line. The Mott-Hubbard phase transition line for the $1/r$ -Hubbard model with $1/r$ -long-range interactions (black solid line) reasonably agrees with the Mott-Hubbard phase transition for the extended $1/r$ -Hubbard model (blue dashed line) when renormalized using the atomic-limit factor $R_{\text{Mott}}^{\text{al}} = \ln 2 \approx 0.693$.

the CDW transition

$$V_{\text{c,ren}}^{\text{CDW}}(U) = \frac{V_{\text{c,NN}}^{\text{CDW}}(U)}{R_{\text{CDW}}} \approx \frac{0.2079 + 0.3675U}{R_{\text{CDW}}} \approx 0.34 + 0.60U \quad (58)$$

The comparison with Eq. (58),

$$V_{\text{c,LR}}^{\text{CDW}}(U) \approx 0.3818 + 0.5293U \approx 0.34 + 0.60U \approx V_{\text{c,ren}}^{\text{CDW}}(U), \quad (59)$$

visualized in Fig. 19, shows that the original and renormalized points for the CDW transition agree within error bars.

2. Mott-Hubbard transition

For the renormalization of the Mott-Hubbard phase transition line, we employ the renormalization factor that occurs in the atomic limit (al), where the kinetic energy is neglected. As shown in the appendix, we have

$$R_{\text{Mott}}^{\text{al}} = \frac{V_{\text{c,NN}}^{\text{al}}(U)}{V_{\text{c,LR}}^{\text{al}}(U)} = \ln 2 \approx 0.693. \quad (60)$$

Evidently, this choice selects the strong-coupling regime as starting point. Therefore, we do not expect perfect results for intermediate couplings, $U \approx W$, where the Mott-Hubbard transition actually occurs.

In Fig. 20 we show the Mott-Hubbard phase transition line for the $1/r$ -Hubbard model with $1/r$ -long-range interactions in comparison with the Mott-Hubbard phase transition for the extended $1/r$ -Hubbard model, renormalized using the atomic-limit factor $R_{\text{Mott}}^{\text{al}} \approx 0.693$.

The two curves agree within error bars, with a systematic deviation of the critical interactions of some 5% for moderate interactions. This is not too surprising because we use only a single number as our renormalization factor. As in the case of the CDW transition, the renormalization is fairly small and very mildly dependent on the Hubbard parameter.

Close to $U = 1$, a linear extrapolation for $V_{\text{c}}^{\text{Mott}}(U)$ according to Eq. (52) gives

$$\begin{aligned} V_{\text{c,NN}}^{\text{Mott}}(U) &= 0.0025 + 5.6269(U - 1) + \mathcal{O}((U - 1)^2), \\ V_{\text{c,LR}}^{\text{Mott}}(U) &= 0.0022 + 6.0106(U - 1) + \mathcal{O}((U - 1)^2). \end{aligned} \quad (61)$$

In linear order, the renormalization factor should be $R_{\text{Mott}}^{\text{lin}} \approx 0.94$ for moderate couplings, instead of $R_{\text{Mott}}^{\text{al}} \approx 0.69$ for strong couplings. The agreement of these factors is still very reasonable, given the fact that moderate couplings $U \approx W$ are far from the strong-coupling limit $U \gg W$.

VI. CONCLUSIONS

In our conclusions, we first summarize our main results. Next, we discuss the relevance of our findings in a broader context.

A. Summary

In this work, we used the SU(2) spin adapted density-matrix renormalization group (DMRG) method for up to $L = 64$ lattice sites and antiperiodic boundary conditions with bond dimension up to $D_{\text{SU}(2)}^{\text{max}} = 6000$ to derive the quantum phase diagram of the one-dimensional $1/r$ -Hubbard model with $1/r$ -long-range interactions at half band-filling. As in our previous publication [23] on the $1/r$ -Hubbard model with nearest-neighbor interactions, we employed the ground-state energy density, the two-particle gap, the structure factor, and the Luttinger parameter to identify the quantum phase transitions between the metallic Luttinger liquid for weak interactions, the Mott-Hubbard insulator for dominant on-site (Hubbard) interactions, and the charge-density wave (CDW) insulator for strong inter-site interactions.

The comparison with the quantum phase diagram for the $1/r$ -Hubbard model with nearest-neighbor interactions leads to two central results:

1. Long-range interactions do not change the quantum phase diagram *qualitatively*.

2. The quantum phase diagrams can *quantitatively* be mapped onto each other by using constant renormalization factors for the quantum phase transition lines.

A model with only nearest-neighbor interactions mimics the long-range model when we put $V_{\text{NN}} \approx R_{\text{qp}} V_{\text{LR}}$ with $R_{\text{qp}} = 0.61 \dots 0.69$. At small interactions, the renormalization factor for the CDW transition, $R_{\text{CDW}} \approx 0.61$, results from Hartree-Fock theory. For large interactions, the atomic limit provides the renormalization factor $R_{\text{Mott}} \approx 0.69$ for the CDW and Mott-Hubbard transitions.

B. Discussion

In this last subsection we discuss the relevance of our findings for interacting many-particle systems. We come to our main conclusion that the inclusion of long-range interactions is not crucial for a proper description of interacting many-electron systems. Therefore, the screening problem is not severe, i.e., long-range interactions can be replaced by effective short-range interactions throughout the ground-state phase diagram with metallic and (Mott) insulating phases.

1. Application to conjugated polymers

Polymers such as poly-acetylene and poly-diacetylene [36, 37] are insulators where the $1/r$ -long-range interaction is only statically screened with a dielectric constant $\varepsilon_d \approx 2.3$. For large electron separations, the long-range interaction must equal the Coulomb interaction,

$$\frac{V_{\text{LR}}}{d/a} = \frac{e^2}{d\varepsilon_d}, \quad (62)$$

where d is the distance between electrons, measured in physical units such as Ångström, $a \approx 1.4$ Å is the average bond-length in trans poly-acetylene, and e is the electronic charge. With the Bohr radius $a_{\text{B}} \approx 0.529$ Å and $E_{\text{Ryd}} = e^2/(2a_{\text{B}}) \approx 13.6$ eV, we have as an estimate for the effective interaction in the extended Hubbard model ($R \approx 0.65$)

$$\begin{aligned} V_{\text{NN}} &= R V_{\text{LR}} = \frac{R}{\varepsilon_d} \frac{2a_{\text{B}}}{a} \frac{e^2}{2a_{\text{B}}} \\ &\approx \frac{0.65}{2.3} \frac{1.06 \text{ Å}}{1.4 \text{ Å}} 13.6 \text{ eV} = 2.9 \text{ eV}. \end{aligned} \quad (63)$$

When the actual zig-zag geometry of poly-acetylene is taken into account [38, 39], the unit cell comprising two carbon atoms has a diameter of $2a = 2.45$ Å which slightly increases the effective nearest-neighbor interaction, $V_{\text{NN}} \approx 3.3$ eV.

A value $V_{\text{NN}} = 3$ eV was successfully applied for the description of the optical properties of poly-acetylene using

the extended Hubbard model [40]. It is thus seen that the factor $R \approx 2/3$ appropriately describes the renormalization of the long-range Coulomb interaction. Note, however, that nowadays long-range Coulomb interactions in fairly long polymers can appropriately be treated using the DMRG method [41, 42].

2. Advantages for numerical investigations

For the same system size, the numerical effort to run DMRG calculations for $1/r$ -long-range interactions scales with system size L , i.e., it is typically about a factor 100 or so higher than for nearest-neighbor interactions. For other numerical approaches such as quantum Monte Carlo (QMC), long-range interactions also pose a major obstacle.

Therefore, it is important to know that a numerical analysis of many-particle systems with short-range interactions is relevant for real systems with long-range Coulomb interactions. Those studies and their results should not be dismissed as irrelevant just because models with short-range interactions are employed.

Moreover, extensive parameter scans can be carried out more easily for models with short-range interactions, e.g., when electron-phonon couplings are included or in the presence of doping. When the region of interest is appropriately narrowed down, the more costly inclusion of long-range Coulomb terms is facilitated using the renormalization factor R_{qp} .

3. Correlation functions

Models with algebraically decaying interactions may display algebraically decaying correlation functions even in the presence of a gap, see, e.g., Ref. [43]. Therefore, it would be interesting to study in detail the behavior of real-space correlation functions close to the quantum phase transitions.

Unfortunately, as seen from Figs. 7 and 8, our systems sizes $L \leq 64$ are too small to address the asymptotic region $L \gg r \gg 1$ where short-range correlations have died out ($r \gg 1$) and finite-size effects are still negligible, $r \ll L$. The Fourier transform of the single-particle density matrix, the momentum distribution $n(k)$, looks discontinuous at first glance despite the fact that it is continuous both in the Luttinger liquid and in the Mott and CDW insulating phases. Likewise, the density-density correlation function $\tilde{C}^{NN}(q)$ looks unspectacular and it is difficult, yet feasible, to extract the Luttinger parameter from it using eq. (30). Much larger systems, of the order of ten thousand sites, are required for a detailed analysis of the asymptotic behavior of real-space correlation functions. Fortunately, for our analysis of the quantum phase diagram, we do not have to rely on correlation functions.

4. Remaining issues

The $1/r$ -Hubbard model is but a single example where the conceptual equivalence of models with short-range and long-range interactions could be tested. Therefore, the question arises: how generic are our findings?

First of all, it should be stated that effective models are frequently and successfully employed in describing low-energy properties of physical systems. For example, s -wave scattering is sufficient for the description of the interaction of slow neutrons with nuclei. A sufficiently strong short-range interaction binds optically excited electrons and holes into excitons in condensed matter theory in the same way as the actual long-range Coulomb interaction. In this sense, it does not come as an utter surprise that the long-range Coulomb interaction can be replaced by an effective short-range interaction in the analysis of physical quantities. The important insight gained from the example of the $1/r$ -Hubbard model lies in the fact that the concept of short-range interactions apparently also applies to the ground-state properties of interacting *many*-particle systems.

Second, we point out that correlations are strongest in one dimension because the particles cannot move around each other. In other words, if screening works in one dimension, it should work even more so in higher dimensions. This ties in with the fact that the Hartree approximation for inter-site interactions becomes exact in the limit of infinite dimensions [44], and it takes modifications to the dynamic mean-field theory (DMFT) [45] to re-introduce inter-site interactions in the limit of high dimensions ('extended' DMFT [46]). We remark in passing that the $1/r$ -Hubbard model might be peculiar in one dimension where nesting is commonplace but nesting of the band structure at half band-filling is rather the exception in higher dimensions.

Finally, we remark that our conclusions are based on a single non-trivial model. More work is necessary to corroborate our findings for other models. As our next testing case, we are currently investigating spinless fermions with $1/r$ -long-range interaction on a half-filled chain for which we recently investigated the CDW transition in the presence of nearest-neighbor interactions [26].

ACKNOWLEDGMENTS

Ö.L. has been supported by the Hungarian National Research, Development, and Innovation Office (NKFIH) through Grant No. K134983, and TKP2021-NVA by the Quantum Information National Laboratory of Hungary. Ö.L. also acknowledges financial support from the Hans Fischer Senior Fellowship program funded by the Technical University of Munich – Institute for Advanced Study and from the Center for Scalable and Predictive methods for Excitation and Correlated phenomena (SPEC), which is funded as part of the Computational Chemical Sciences Program FWP 70942 by the U.S. Department of

Energy (DOE), Office of Science, Office of Basic Energy Sciences, Division of Chemical Sciences, Geosciences, and Biosciences at Pacific Northwest National Laboratory.

Appendix: Hartree-Fock theory

In this appendix we derive the Hartree-Fock theory for the one-dimensional $1/r$ -Hubbard model with $1/r$ -long-range interactions at half band-filling when a Fermi-liquid phase competes with a charge-density-wave phase.

1. CDW Hartree-Fock Hamiltonian

In Hartree-Fock theory, we decouple the Hubbard interaction as follows,

$$\hat{D}^{\text{HF}} = \hat{D}^{\text{H}} = \sum_l \left[\langle \hat{n}_{l,\uparrow} \rangle \hat{n}_{l,\downarrow} + \hat{n}_{l,\uparrow} \langle \hat{n}_{l,\downarrow} \rangle - \langle \hat{n}_{l,\uparrow} \rangle \langle \hat{n}_{l,\downarrow} \rangle \right]. \quad (\text{A.1})$$

For the long-range terms, we have Hartree and Fock contributions,

$$\hat{V}^{\text{HF}} = \hat{V}^{\text{H}} + \hat{V}^{\text{F}}, \quad (\text{A.2})$$

with

$$\begin{aligned} \hat{V}^{\text{H}} = V \sum_{r=1}^{L/2} V(r) \sum_{l=1}^L & \left[(\langle \hat{n}_l \rangle - 1) (\hat{n}_{l+r} - 1) \right. \\ & + (\hat{n}_l - 1) (\langle \hat{n}_{l+r} \rangle - 1) \\ & \left. - (\langle \hat{n}_l \rangle - 1) (\langle \hat{n}_{l+r} \rangle - 1) \right] \quad (\text{A.3}) \end{aligned}$$

and

$$\begin{aligned} \hat{V}^{\text{F}} = V \sum_{r=1}^{L/2} V(r) \sum_{l=1, \sigma}^L & \left[\langle \hat{c}_{l,\sigma}^+ \hat{c}_{l+r,\sigma} \rangle \hat{c}_{l,\sigma} \hat{c}_{l+r,\sigma}^+ \right. \\ & + \hat{c}_{l,\sigma}^+ \hat{c}_{l+r,\sigma} \langle \hat{c}_{l,\sigma} \hat{c}_{l+r,\sigma}^+ \rangle \\ & \left. - \langle \hat{c}_{l,\sigma}^+ \hat{c}_{l+r,\sigma} \rangle \langle \hat{c}_{l,\sigma} \hat{c}_{l+r,\sigma}^+ \rangle \right] \quad (\text{A.4}) \end{aligned}$$

Here, $\langle \hat{A} \rangle$ denotes the ground-state expectation value of the operator \hat{A} , $\langle \hat{A} \rangle \equiv \langle \Phi_0 | \hat{A} | \Phi_0 \rangle$, with $|\Phi_0\rangle$ as the ground state of the Hartree-Fock Hamiltonian \hat{H}^{HF} , see below.

We make the CDW Ansatz for the order parameter

$$\langle \hat{n}_{l,\sigma} \rangle = \frac{1}{2} (1 + (-1)^l \Delta) \quad (\text{A.5})$$

with the real CDW parameter $\Delta \geq 0$. This Ansatz implies that the unit cell has doubled.

Furthermore, we introduce the abbreviation ($r \neq 0$)

$$B_r(l) = \langle \hat{c}_{l,\sigma}^+ \hat{c}_{l+r,\sigma} \rangle = i b_r(l). \quad (\text{A.6})$$

Particle-hole symmetry implies that $B_r(l)$ is purely complex at half band-filling,

$$B_r^*(l) = \langle \hat{c}_{l+r,\sigma}^+ \hat{c}_{l,\sigma} \rangle = \langle \hat{c}_{l+r,\sigma} \hat{c}_{l,\sigma}^+ \rangle = -B_r(l), \quad (\text{A.7})$$

where we used particle-hole symmetry in the second step. Therefore, $b_r(l)$ is real. Since the unit cell has doubled, we make the Ansatz that $b_r(l)$ alternates just as the local order parameter,

$$b_r(l) = b_r + (-1)^l d_r, \quad (\text{A.8})$$

allowing thus for a bond-order wave.

With these abbreviations, we can rewrite the Hartree-Fock interaction at half band-filling as

$$\hat{D}^{\text{H}} = \frac{L}{4} (1 - \Delta^2) + \frac{\Delta}{2} \sum_{l,\sigma} (-1)^l \hat{n}_{l,\sigma}, \quad (\text{A.9})$$

$$\hat{V}^{\text{H}} = -L\Delta^2 \bar{V} + 2\Delta \bar{V} \sum_{l=1,\sigma}^L (-1)^l \hat{n}_{l,\sigma}, \quad (\text{A.10})$$

$$\bar{V} = V \sum_{r=1}^{L/2} (-1)^r V(r), \quad (\text{A.11})$$

and

$$\begin{aligned} \hat{V}^{\text{F}} = 2LV \sum_{r=1}^{L/2} V(r) & (b_r^2 + d_r^2) \\ & + V \sum_{r=1}^{L/2} V(r) b_r \sum_{l=1,\sigma}^L i [\hat{c}_{l,\sigma}^+ \hat{c}_{l+r,\sigma} - \hat{c}_{l+r,\sigma}^+ \hat{c}_{l,\sigma}] \\ & + V \sum_{r=1}^{L/2} V(r) d_r \sum_{l=1,\sigma}^L (-1)^l i [\hat{c}_{l,\sigma}^+ \hat{c}_{l+r,\sigma} - \hat{c}_{l+r,\sigma}^+ \hat{c}_{l,\sigma}]. \quad (\text{A.12}) \end{aligned}$$

The resulting single-particle problem defines the Hartree-Fock Hamiltonian for a possible CDW ground state

$$\hat{H}^{\text{HF}} = \hat{T} + U \hat{D}^{\text{H}} + \hat{V}^{\text{H}} + \hat{V}^{\text{F}}. \quad (\text{A.13})$$

It has to be solved self-consistently, i.e., the parameters Δ , b_r and d_r must be chosen such that the ground state fulfills Eqs. (A.5) and (A.6).

2. Diagonalization of the Hartree-Fock Hamiltonian

In the CDW phase, the Hartree-Fock Hamiltonian is identical for both spin species, $\hat{H}^{\text{HF}} = \sum_{\sigma} \hat{H}_{\sigma}^{\text{HF}}$. Drop-

ping the spin index we must diagonalize

$$\begin{aligned}\hat{H}_{\text{sf}} = & \sum_k \epsilon(k) \hat{C}_k^+ \hat{C}_k + \left(\frac{U}{2} + 2\bar{V} \right) \Delta \sum_l (-1)^l \hat{n}_l + C \\ & + V \sum_{r=1}^{L/2} V(r) b_r \sum_{l=1}^L i [\hat{c}_l^+ \hat{c}_{l+r} - \hat{c}_{l+r}^+ \hat{c}_l] \\ & + V \sum_{r=1}^{L/2} V(r) d_r \sum_{l=1}^L (-1)^l i [\hat{c}_l^+ \hat{c}_{l+r} - \hat{c}_{l+r}^+ \hat{c}_l]\end{aligned}\quad (\text{A.14})$$

for spinless fermions ('sf'), where

$$C = L \frac{U}{8} (1 - \Delta^2) - L \frac{\bar{V} \Delta^2}{2} + LV \sum_{r=1}^{L/2} V(r) (b_r^2 + d_r^2) . \quad (\text{A.15})$$

In momentum space, the Hamiltonian reads

$$\begin{aligned}\hat{H}_{\text{sf}} = & C + \sum_k' \left[(\epsilon(k) + b_e(k)) \hat{C}_k^+ \hat{C}_k \right. \\ & \left. + (\epsilon(k + \pi) + b_o(k)) \hat{C}_{k+\pi}^+ \hat{C}_{k+\pi} \right] \\ & + \left(\frac{U}{2} + 2\bar{V} \right) \Delta \sum_k' \left(\hat{C}_k^+ \hat{C}_{k+\pi} + \hat{C}_{k+\pi}^+ \hat{C}_k \right) \\ & + \sum_k' \left(d(k) \hat{C}_k^+ \hat{C}_{k+\pi} + d^*(k) \hat{C}_{k+\pi}^+ \hat{C}_k \right) \quad (\text{A.16})\end{aligned}$$

where the prime on the sum indicates the k -space region $-\pi < k < 0$.

Moreover, we introduced the abbreviations

$$\begin{aligned}b_e(k) &= -2V \sum_{r=1}^{L/2} V(r) b_r \sin(kr) , \\ b_o(k) &= -2V \sum_{r=1}^{L/2} (-1)^r V(r) b_r \sin(kr) , \quad (\text{A.17})\end{aligned}$$

and

$$\begin{aligned}d(k) &= V \sum_{r=1}^{L/2} i V(r) d_r ((-1)^r e^{ikr} - e^{-ikr}) \\ &= d_R(k) + i d_I(k) , \\ d_R(k) &= -V \sum_{r=1}^{L/2} V(r) d_r (1 + (-1)^r) \sin(kr) , \\ d_I(k) &= -V \sum_{r=1}^{L/2} V(r) d_r (1 - (-1)^r) \cos(kr) .\end{aligned}\quad (\text{A.18})$$

We diagonalize \hat{H}_{sf} with the help of the linear transformation

$$\begin{aligned}\hat{C}_k &= c_k \hat{\alpha}_k - s_k e^{i\psi_k} \hat{\beta}_k , \\ \hat{C}_{k+\pi} &= s_k e^{-i\psi_k} \hat{\alpha}_k + c_k \hat{\beta}_k ,\end{aligned}\quad (\text{A.19})$$

where we abbreviate $c_k \equiv \cos(\varphi_k)$ and $s_k = \sin(\varphi_k)$, and φ_k and ψ_k are real phases. For each $-\pi < k < 0$, \hat{h}_k must be diagonal in the new operators where

$$\begin{aligned}\hat{h}_k = & (\epsilon(k) + b_e(k)) \\ & \times \left(c_k \hat{\alpha}_k^+ - s_k e^{-i\psi_k} \hat{\beta}_k^+ \right) \left(c_k \hat{\alpha}_k - s_k e^{i\psi_k} \hat{\beta}_k \right) \\ & + (\epsilon(k + \pi) + b_o(k)) \\ & \times \left(s_k e^{i\psi_k} \hat{\alpha}_k^+ + c_k \hat{\beta}_k^+ \right) \left(s_k e^{-i\psi_k} \hat{\alpha}_k + c_k \hat{\beta}_k \right) \\ & + \left(\frac{U\Delta}{2} + 2\bar{V}\Delta + d(k) \right) \\ & \times \left(c_k \hat{\alpha}_k^+ - s_k e^{-i\psi_k} \hat{\beta}_k^+ \right) \left(s_k e^{-i\psi_k} \hat{\alpha}_k + c_k \hat{\beta}_k \right) \\ & + \left(\frac{U\Delta}{2} + 2\bar{V}\Delta + d^*(k) \right) \\ & \times \left(s_k e^{i\psi_k} \hat{\alpha}_k^+ + c_k \hat{\beta}_k^+ \right) \left(c_k \hat{\alpha}_k - s_k e^{i\psi_k} \hat{\beta}_k \right) .\end{aligned}\quad (\text{A.20})$$

The mixed terms proportional to $\hat{\alpha}_k^+ \hat{\beta}_k$ in \hat{h}_k read

$$\begin{aligned}M_k = & (\epsilon(k) + b_e(k)) (-c_k s_k e^{i\psi_k}) \\ & + (\epsilon(k + \pi) + b_o(k)) (c_k s_k e^{i\psi_k}) \\ & + \left(\frac{U\Delta}{2} + 2\bar{V}\Delta + d(k) \right) c_k^2 \\ & + \left(\frac{U\Delta}{2} + 2\bar{V}\Delta + d^*(k) \right) (-s_k^2 e^{2i\psi_k}) .\end{aligned}\quad (\text{A.21})$$

We demand that the mixing term vanishes, $M_k = 0 = M_k^*$, which implies

$$\begin{aligned}\text{lhs} &= \text{rhs} , \\ \text{lhs} &= \sin(2\varphi_k) (\epsilon(k) - \epsilon(k + \pi) + b_e(k) - b_o(k)) , \\ \text{rhs} &= \left(\frac{U\Delta}{2} + 2\bar{V}\Delta + d(k) \right) e^{-i\psi_k} \cos(2\varphi_k) \\ &+ \left(\frac{U\Delta}{2} + 2\bar{V}\Delta + d^*(k) \right) e^{i\psi_k} \cos(2\varphi_k) \\ &+ \left(\frac{U\Delta}{2} + 2\bar{V}\Delta + d(k) \right) e^{-i\psi_k} \\ &- \left(\frac{U\Delta}{2} + 2\bar{V}\Delta + d^*(k) \right) e^{i\psi_k} \\ &= 2 \cos(2\varphi_k) \left(\frac{U\Delta}{2} + 2\bar{V}\Delta + d_R(k) \right) \cos(\psi_k) \\ &+ 2 \cos(2\varphi_k) d_I(k) \sin(\psi_k) \\ &- 2i \left(\frac{U\Delta}{2} + 2\bar{V}\Delta + d_R(k) \right) \sin(\psi_k) \\ &+ 2i d_I(k) \cos(\psi_k) ,\end{aligned}\quad (\text{A.22})$$

where we used Eq. (A.18) and

$$\begin{aligned} c_k^2 &= \frac{1}{2} (1 + \cos(2\varphi_k)) , \\ s_k^2 &= \frac{1}{2} (1 - \cos(2\varphi_k)) , \\ c_k s_k &= \frac{1}{2} \sin(2\varphi_k) . \end{aligned} \quad (\text{A.23})$$

Apparently, the imaginary terms of the right-hand-side of eq. (A.22) must vanish, which leads to

$$\tan(\psi_k) = \frac{2d_I(k)}{U\Delta + 4\bar{V}\Delta + 2d_R(k)} \quad (\text{A.24})$$

for the phase ψ_k . Moreover, the real part of the eq. (A.22) leads to

$$\begin{aligned} \tan(2\varphi_k) &= \frac{[-Z(k)]}{\epsilon(k) - \epsilon(k + \pi) + b_e(k) - b_o(k)} \geq 0 , \\ Z(k) &= -(U\Delta + 4\bar{V}\Delta + 2d_R(k)) \cos(\psi_k) \\ &\quad - 2d_I(k) \sin(\psi_k) \\ &= \sqrt{(U\Delta + 4\bar{V}\Delta + 2d_R(k))^2 + 4[d_I(k)]^2} , \end{aligned} \quad (\text{A.25})$$

where we assumed that $U\Delta + 4\bar{V}\Delta + 2d_R(k) < 0$. The diagonal terms give

$$h_k = E_\alpha(k) \hat{\alpha}_k^+ \hat{\alpha}_k + E_\beta(k) \hat{\beta}_k^+ \hat{\beta}_k \quad (\text{A.26})$$

with

$$\begin{aligned} E_\alpha(k) &= (\epsilon(k) + b_e(k)) c_k^2 + (\epsilon(k + \pi) + b_o(k)) s_k^2 \\ &\quad + \left(\frac{U\Delta}{2} + 2\bar{V}\Delta + d(k) \right) e^{-i\psi_k} c_k s_k \\ &\quad + \left(\frac{U\Delta}{2} + 2\bar{V}\Delta + d^*(k) \right) e^{i\psi_k} c_k s_k \\ &= \frac{1}{2} [\epsilon(k) + \epsilon(k + \pi) + b_e(k) + b_o(k)] - s(k) , \\ E_\beta(k) &= \frac{1}{2} [\epsilon(k) + \epsilon(k + \pi) + b_e(k) + b_o(k)] + s(k) , \end{aligned} \quad (\text{A.27})$$

where

$$\begin{aligned} s(k) &= \frac{1}{2} \sqrt{[Z(k)]^2 + [\epsilon(k) - \epsilon(k + \pi) + b_e(k) - b_o(k)]^2} \\ &= \frac{1}{2} \left[(U\Delta + 4\bar{V}\Delta + 2d_R(k))^2 + 4[d_I(k)]^2 \right. \\ &\quad \left. + [\epsilon(k) - \epsilon(k + \pi) + b_e(k) - b_o(k)]^2 \right]^{1/2} \end{aligned} \quad (\text{A.28})$$

The Hartree-Fock Hamiltonian becomes diagonal with the quasi-particle dispersion $E_{\alpha,\beta}(k)$,

$$\hat{H}^{\text{HF}} = 2C + \sum_{k,\sigma}' \left[E_\alpha(k) \hat{\alpha}_{k,\sigma}^+ \hat{\alpha}_{k,\sigma} + E_\beta(k) \hat{\beta}_{k,\sigma}^+ \hat{\beta}_{k,\sigma} \right] , \quad (\text{A.29})$$

where we re-introduced the spin index. Since $E_\alpha(k) < E_\beta(k)$ for all $-\pi < k < 0$, the ground state at half band-filling contains only α -particles,

$$|\Phi_0\rangle = \prod_{-\pi < k < 0, \sigma} \hat{\alpha}_{k,\sigma}^+ |\text{vac}\rangle . \quad (\text{A.30})$$

3. Self-consistency equations and CDW transition

The self-consistency equation (A.5) becomes

$$\begin{aligned} \Delta &= \frac{1}{L} \sum_k' \langle \hat{C}_{k,\sigma}^+ \hat{C}_{k+\pi,\sigma} + \hat{C}_{k+\pi,\sigma}^+ \hat{C}_{k,\sigma} \rangle \\ &= \frac{1}{L} \sum_k' \sin(2\varphi_k) \cos(\psi_k) \\ &= -\frac{1}{L} \sum_k' \frac{[U\Delta/2 + 2\bar{V}\Delta + d_R(k)]}{s(k)} \\ &= -\int_{-\pi}^0 \frac{dk}{2\pi} \frac{[U\Delta/2 + 2\bar{V}\Delta + d_R(k)]}{s(k)} \end{aligned} \quad (\text{A.31})$$

in the thermodynamic limit. The self-consistency equation (A.6) for the bond dimerization becomes

$$\begin{aligned} ib_r + (-1)^l id_r &= \frac{1}{L} \sum_k e^{-ikl} e^{ik(l+r)} \langle \hat{C}_{k,\sigma}^+ \hat{C}_{k,\sigma} \rangle \\ &\quad + \frac{1}{L} \sum_k e^{-ikl} e^{i(k+\pi)(l+r)} \langle \hat{C}_{k,\sigma}^+ \hat{C}_{k+\pi,\sigma} \rangle \end{aligned} \quad (\text{A.32})$$

so that

$$ib_r = \frac{1}{L} \sum_k' e^{ikr} \left[\langle \hat{C}_{k,\sigma}^+ \hat{C}_{k,\sigma} \rangle + (-1)^r \langle \hat{C}_{k+\pi,\sigma}^+ \hat{C}_{k+\pi,\sigma} \rangle \right] \quad (\text{A.33})$$

and

$$id_r = \frac{1}{L} \sum_k' e^{ikr} \left[(-1)^r \langle \hat{C}_{k,\sigma}^+ \hat{C}_{k+\pi,\sigma} \rangle + \langle \hat{C}_{k+\pi,\sigma}^+ \hat{C}_{k,\sigma} \rangle \right] . \quad (\text{A.34})$$

This results in

$$\begin{aligned} ib_r &= \frac{(1 - (-1)^r)}{2} i\tilde{b}_r , \\ i\tilde{b}_r &= -\frac{1}{L} \sum_k' e^{ikr} \frac{[\epsilon(k) - \epsilon(k + \pi) + b_e(k) - b_o(k)]}{2s(k)} , \\ \tilde{b}_r &= -\int_{-\pi}^0 \frac{dk}{2\pi} \sin(kr) \frac{[\epsilon(k) - \epsilon(k + \pi) + b_e(k) - b_o(k)]}{2s(k)} \end{aligned} \quad (\text{A.35})$$

in the thermodynamic limit. Here, we used that b_r is real. Note that $b_r \neq 0$ only for odd distances, $r = 2m+1$. From

eq. (A.18) it thus follows that $b(k) \equiv b_e(k) = -b_o(k)$ with

$$b(k) = -2V \sum_{r=1}^{L/2} V(r) \tilde{b}_r \frac{(1 - (-1)^r)}{2} \sin(kr), \quad (\text{A.36})$$

$$\tilde{b}_r = - \int_{-\pi}^0 \frac{dk}{2\pi} \sin(kr) \frac{[\epsilon(k) - \epsilon(k + \pi) + 2b(k)]}{2s(k)}$$

with

$$s(k) = \frac{1}{2} \left[(U\Delta + 4\bar{V}\Delta + 2d_R(k))^2 + 4[d_I(k)]^2 + [\epsilon(k) - \epsilon(k + \pi) + 2b(k)]^2 \right]^{1/2}. \quad (\text{A.37})$$

The dispersion relation thus simplifies to

$$E_\alpha(k) = \frac{1}{2} [\epsilon(k) + \epsilon(k + \pi)] - s(k),$$

$$E_\beta(k) = \frac{1}{2} [\epsilon(k) + \epsilon(k + \pi)] + s(k). \quad (\text{A.38})$$

Furthermore, eq. (A.34) leads to

$$\text{id}_r = \frac{1}{L} \sum_k' e^{ikr} c_k s_k [(-1)^r e^{-i\psi_k} + e^{i\psi_k}] \quad (\text{A.39})$$

$$d_r = \frac{1 - (-1)^r}{2} d_{r,o} + \frac{1 + (-1)^r}{2} d_{r,e},$$

$$d_{r,o} = \frac{1}{L} \sum_k' 2c_k s_k \cos(kr) \sin \psi_k$$

$$= - \int_{-\pi}^0 \frac{dk}{2\pi} \cos(kr) \frac{d_I(k)}{s(k)},$$

$$d_{r,e} = \frac{1}{L} \sum_k' 2c_k s_k \sin(kr) \cos \psi_k$$

$$= - \int_{-\pi}^0 \frac{dk}{2\pi} \sin(kr) \frac{U\Delta/2 + 2\bar{V}\Delta + d_R(k)}{s(k)}.$$

Recall that

$$d_R(k) = -V \sum_{r=1}^{L/2} V(r) d_{r,e} (1 + (-1)^r) \sin(kr),$$

$$d_I(k) = -V \sum_{r=1}^{L/2} V(r) d_{r,o} (1 - (-1)^r) \cos(kr). \quad (\text{A.40})$$

When we only have a nearest-neighbor interaction, i.e., $V(r) = \delta_{r,1}$, the set $\{d_R(k) = 0, d_{r,o} = 0\}$ provides a self-consistent solution and we recover the equations given in Ref. [23].

4. Purely real dimerization function

As a convenient simplification, we will search solutions for a purely real dimerization, $d_{r,o} = 0$. Eq. (A.40) shows

that the Ansatz $d_{r,o} = 0$ leads to $d_I(k) = 0$. When inserted in eq. (A.39), we recover $d_{r,o} = 0$. Self-consistency is achieved, irrespective of all other variational parameters. It implies that

$$\psi_k = 0 \quad (\text{A.41})$$

and

$$Z(k) = -[U\Delta + 4\bar{V}\Delta + 2d(k)]. \quad (\text{A.42})$$

The self-consistency equations simplify to

$$\Delta = - \int_{-\pi}^0 \frac{dk}{2\pi} \frac{[U\Delta/2 + 2\bar{V}\Delta + d(k)]}{s(k)},$$

$$b(k) = -2V \sum_{r=1}^{L/2} V(r) \tilde{b}_r \frac{(1 - (-1)^r)}{2} \sin(kr),$$

$$\tilde{b}_r = - \int_{-\pi}^0 \frac{dk}{2\pi} \sin(kr) \frac{[\epsilon(k) - \epsilon(k + \pi) + 2b(k)]}{2s(k)},$$

$$d(k) = -V \sum_{r=1}^{L/2} V(r) d_r (1 + (-1)^r) \sin(kr),$$

$$d_r = - \int_{-\pi}^0 \frac{dk}{2\pi} \sin(kr) \frac{U\Delta/2 + 2\bar{V}\Delta + d(k)}{s(k)} \quad (\text{A.43})$$

where

$$s(k) = -\frac{1}{2} \left[(U\Delta + 4\bar{V}\Delta + 2d(k))^2 + [\epsilon(k) - \epsilon(k + \pi) + 2b(k)]^2 \right]^{1/2} \quad (\text{A.44})$$

Recall that the parameters \tilde{b}_r are defined only for odd r , and the parameters d_r are defined only for even r .

The self-consistency equations show that, (i), the Coulomb interaction at odd particle distances influences the charge-density-wave order, and, (ii), the Coulomb interaction at even distances can trigger a bond-order-wave instability.

5. Minimization of the Hartree-Fock ground-state energy

As an alternative to the solution of the self-consistency equations, we can also address the Hartree-Fock ground-state energy per spin species,

$$\frac{e_0^{\text{HF}}(U, V)}{2} = \frac{C}{L} + \int_{-\pi}^0 \frac{dk}{2\pi} \left[\frac{1}{2} [\epsilon(k) + \epsilon(k + \pi)] - s(k) \right] \quad (\text{A.45})$$

with

$$\frac{C}{L} = \frac{U}{8} (1 - \Delta^2) - \frac{\bar{V}\Delta^2}{2} \quad (\text{A.46})$$

$$+ V \sum_{r=1}^{L/2} V(r) \left[\frac{(1 - (-1)^r)}{2} \tilde{b}_r^2 + \frac{(1 + (-1)^r)}{2} d_r^2 \right],$$

where we used eqs. (A.15) and (A.38) for a purely real dimerization function. From eq. (A.44) we have

$$s(k) = \frac{1}{2} \left[(U\Delta + 4\bar{V}\Delta + 2d(k))^2 + [\epsilon(k) - \epsilon(k + \pi) + 2b(k)]^2 \right]^{1/2}, \quad (\text{A.47})$$

where

$$b(k) = -V \sum_{r=1}^{L/2} V(r) \tilde{b}_r (1 - (-1)^r) \sin(kr),$$

$$d(k) = -V \sum_{r=1}^{L/2} V(r) d_r (1 + (-1)^r) \sin(kr). \quad (\text{A.48})$$

Recall that

$$\bar{V} = V \sum_{r=1}^{L/2} (-1)^r V(r) < 0. \quad (\text{A.49})$$

The task is to minimize the Hartree-Fock ground-state energy $e_0^{\text{HF}}(U, V)$ with respect to the variational parameters Δ , \tilde{b}_r (r : odd), and d_r ; r is even.

6. CDW critical interaction for weak coupling

In the absence of bond order, $d(k) = 0$ and $d_r = 0$, the critical interaction strength is obtained from putting $\Delta = 0^+$ in the above equations. We thereby assume a continuous transition, which is the case for $U, V \lesssim W$. We then have

$$s(k) = -\frac{1}{2} (\epsilon(k) - \epsilon(k + \pi) + 2b_c(k)) \quad (\text{A.50})$$

for $-\pi < k < 0$. Thus, with Δ from Eq. (A.43),

$$1 = \int_{-\pi}^0 \frac{dk}{\pi} \frac{U/2 + 2\bar{V}_c}{1/2 [\epsilon(k) - \epsilon(k + \pi) + 2b_c(k)]}, \quad (\text{A.51})$$

where $\epsilon(k) - \epsilon(k + \pi) = -\pi t$ and

$$b_c(k) = -2V_{c,\text{LR}} \sum_{r=1}^{\infty} V(r) \tilde{b}_r \left(\frac{1 - (-1)^r}{2} \right) \sin(kr)$$

$$= \frac{2V_{c,\text{LR}}}{\pi} B(k),$$

$$B(k) = \sum_{m=0}^{\infty} \frac{\sin((2m+1)k)}{(2m+1)^2}, \quad (\text{A.52})$$

because

$$\tilde{b}_r = - \int_{-\pi}^0 \frac{dk}{2\pi} \sin(kr) \frac{\epsilon(k) - \epsilon(k + \pi) + 2b(k)}{2s(k)}$$

$$= \int_{-\pi}^0 \frac{dk}{2\pi} \sin(kr) = -\frac{1}{2\pi r} (1 - (-1)^r) \quad (\text{A.53})$$

in the thermodynamic limit. With $\bar{V} = -V_{c,\text{LR}} \ln 2$ from

$$\sum_{r=1}^{\infty} \frac{(-1)^r}{r} = \ln 2, \quad (\text{A.54})$$

$V_{c,\text{LR}}$ results from

$$1 = \int_0^{\pi} \frac{dk}{\pi} \frac{4V_{c,\text{LR}} \ln 2 - U}{W/2 + 4V_{c,\text{LR}} B(k)/\pi}, \quad (\text{A.55})$$

where $B(k) \geq 0$ for $0 \leq k \leq \pi$. Thus, $V_{c,\text{LR}} > U/(4 \ln 2)$ is a condition.

For small U and with $V_{c,\text{LR}} = a_{\text{LR}} + Ub_{\text{LR}}$, we find

$$1 = \int_0^{\pi} dk \frac{8a_{\text{LR}} \ln 2}{8a_{\text{LR}} B(k) + \pi}, \quad (\text{A.56})$$

which leads to $a_{\text{LR}} \approx 0.255298$ to leading order. To first order, we have

$$\frac{1}{b_{\text{LR}}} = 32\pi (\ln 2)^2 a_{\text{LR}} \int_0^{\pi} \left(\frac{1}{8a_{\text{LR}} B(k) + \pi} \right)^2, \quad (\text{A.57})$$

so that we find $b_{\text{LR}} \approx 0.502707$.

For the case of nearest-neighbor interactions, the same analysis gives, see Eq. (A22) of Ref. [23],

$$\frac{1}{\alpha_c - 2U/\pi} = \frac{\pi}{\sqrt{1 - \alpha_c^2}} - \frac{2}{\sqrt{1 - \alpha_c^2}} \arctan \left(\frac{\alpha_c}{\sqrt{1 - \alpha_c^2}} \right) \quad (\text{A.58})$$

with the abbreviation $\alpha_c = 8V_{c,\text{NN}}/\pi$. This equation must be solved numerically for given U .

For weak Hubbard interactions, we set

$$\alpha_c(U) = \alpha_0 + \alpha_1 U \quad (\text{A.59})$$

to find $\alpha_0 \approx 0.394235$ so that $V_{c,\text{NN}}^{\text{HF}}(U = 0) \approx 0.154816 = a_{\text{NN}}^{\text{HF}}$. Moreover,

$$\alpha_1 = 2(1 - \alpha_0^2)/[\pi(1 - 2\alpha_0^2)], \quad (\text{A.60})$$

so that $\alpha_1 \approx 0.780192$ and $b_{\text{NN}}^{\text{HF}} \approx 0.306381$ for the CDW transition for the extended $1/r$ -Hubbard model in Hartree-Fock theory.

7. CDW critical interaction in the atomic limit

Since the transition is discontinuous for strong interactions, we must compare the ground-state energies of the CDW and non-ordered phases directly.

In the atomic limit, we can ignore the contribution of the kinetic energy and may focus on the disordered state with one electron per site that has the energy $E_{\text{dis}} = 0$. In comparison, the CDW state, with double occupancies on even lattice sites and holes on odd sites, has the energy

$$E_{\text{NN}}^{\text{CDW}} = \frac{L}{2} U + L(-V),$$

$$E_{\text{LR}}^{\text{CDW}} = \frac{L}{2} U + L \sum_{r=1}^{L/2} V \frac{(-1)^r}{d(r)} \quad (\text{A.61})$$

for nearest-neighbor interactions and $1/r$ -long-range interactions. Using eq. (A.54) we thus find for the extended Hubbard model

$$e_{\text{NN}}^{\text{CDW}} = \frac{U}{2} - V \quad (\text{A.62})$$

and

$$e_{\text{LR}}^{\text{CDW}} = \frac{U}{2} - V \ln(2) \quad (\text{A.63})$$

for the Hubbard model with $1/r$ -long-range interactions, respectively.

In the atomic limit, $\hat{T} \equiv 0$, the CDW transitions occur at $V_{\text{c,NN}}^{\text{al}}(U) = U/2$ for the extended Hubbard model and

at $V_{\text{c,LR}}^{\text{al}}(U) = U/(2 \ln(2))$ for the Hubbard model with $1/r$ -long-range interactions, respectively. These considerations justify the phase separation lines in Fig. 1.

Moreover, the renormalization factor that maps the ground-state energies onto each other is given by

$$R^{\text{Mott}}(U, V \gg W) = \frac{V_{\text{c,NN}}^{\text{al}}(U)}{V_{\text{c,LR}}^{\text{al}}(U)} = \ln(2). \quad (\text{A.64})$$

This factor is used in the renormalization of the critical line for the Mott transition.

-
- [1] A. L. Fetter and J. D. Walecka, *Quantum Theory of Many-Particle Systems*, 7th ed. (Dover, 2003).
 - [2] G. D. Mahan, *Many particle physics*, 3rd ed. (Kluwer Academic/Plenum, New York, Boston, 2007).
 - [3] J. W. Negele and H. Orland, *Quantum Many-Particle Systems* (Addison-Wesley, Redwood City, 1988).
 - [4] N. F. Mott, The basis of the electron theory of metals, with special reference to the transition metals, *Proceedings of the Physical Society. Section A* **62**, 416 (1949).
 - [5] N. F. Mott, *Metal-Insulator Transitions*, 2nd ed. (Taylor & Francis, London, 1990).
 - [6] F. Gebhard, *The Mott Metal-Insulator Transition*, Springer Tracts in Modern Physics, Vol. **137** (Springer, Berlin, Heidelberg, 1997).
 - [7] J. Sólyom, *Fundamentals of the Physics of Solids* (Springer, Berlin, 2009) vol. 3.
 - [8] J. Hubbard, Electron Correlations in Narrow Energy Bands, *Proc. Royal Soc. A* **276**, 238 (1963).
 - [9] M. Gutzwiller, Effect of correlation on the ferromagnetism of transition metals, *Phys. Rev. Lett.* **10**, 159 (1963).
 - [10] J. Kanamori, Electron Correlation and Ferromagnetism of Transition Metals, *Prog. Theor. Phys.* **30**, 275 (1963).
 - [11] E. H. Lieb and F. Y. Wu, Absence of Mott transition in an Exact Solution of the Short-Range, One-Band Model in One Dimension, *Phys. Rev. Lett.* **21**, 192 (1968).
 - [12] F. H. L. Essler, H. Frahm, F. Göhmann, A. Klümper, and V. E. Korepin, *The One-Dimensional Hubbard Model* (Cambridge University Press, 2005).
 - [13] P. W. Anderson, New approach to the theory of superexchange interactions, *Phys. Rev.* **115**, 2 (1959).
 - [14] F. H. L. Essler, F. Gebhard, and E. Jeckelmann, Excitons in one-dimensional Mott insulators, *Phys. Rev. B* **64**, 125119 (2001).
 - [15] P. G. J. van Dongen, Extended Hubbard model at weak coupling, *Phys. Rev. B* **50**, 14016 (1994).
 - [16] P. G. J. van Dongen, Extended Hubbard model at strong coupling, *Phys. Rev. B* **49**, 7904 (1994).
 - [17] T. Giamarchi, *Quantum Physics in One Dimension* (Clarendon Press, Oxford, 2004).
 - [18] S. B. Dugdale, Life on the edge: a beginner's guide to the Fermi surface, *Physica Scripta* **91**, 053009 (2016).
 - [19] M. D. Johannes and I. I. Mazin, Fermi surface nesting and the origin of charge density waves in metals, *Phys. Rev. B* **77**, 165135 (2008).
 - [20] F. Gebhard and A. E. Ruckenstein, Exact results for a Hubbard chain with long-range hopping, *Phys. Rev. Lett.* **68**, 244 (1992).
 - [21] F. Gebhard, A. Girndt, and A. E. Ruckenstein, Charge- and spin-gap formation in exactly solvable Hubbard chains with long-range hopping, *Phys. Rev. B* **49**, 10926 (1994).
 - [22] F. Gebhard and Ö. Legeza, Tracing the Mott-Hubbard transition in one-dimensional Hubbard models without Umklapp scattering, *Phys. Rev. B* **104**, 245118 (2021).
 - [23] F. Gebhard, K. Bauerbach, and Ö. Legeza, Generic Mott-Hubbard phase diagram for extended Hubbard models without Umklapp scattering, *Phys. Rev. B* **108**, 205130 (2023).
 - [24] W. Li, A. Dhar, X. Deng, K. Kasamatsu, L. Barbiero, and L. Santos, Disorderless quasi-localization of polar gases in one-dimensional lattices, *Phys. Rev. Lett.* **124**, 010404 (2020).
 - [25] C. Cheng, Many-body localization in clean chains with long-range interactions, *Phys. Rev. B* **108**, 155113 (2023).
 - [26] F. Gebhard, K. Bauerbach, and Ö. Legeza, Accurate localization of Kosterlitz-Thouless-type quantum phase transitions for one-dimensional spinless fermions, *Phys. Rev. B* **106**, 205133 (2022).
 - [27] S. R. White, Density matrix formulation for quantum renormalization groups, *Phys. Rev. Lett.* **69**, 2863 (1992).
 - [28] U. Schollwöck, The Density-Matrix Renormalization Group, *Rev. Mod. Phys.* **77**, 259 (2005).
 - [29] H. J. Schulz, Correlation exponents and the metal-insulator transition in the one-dimensional Hubbard model, *Phys. Rev. Lett.* **64**, 2831 (1990).
 - [30] T. Giamarchi and H. J. Schulz, Correlation functions of one-dimensional quantum systems, *Phys. Rev. B* **39**, 4620 (1989).
 - [31] S. Ejima, F. Gebhard, and S. Nishimoto, Tomonaga-Luttinger parameters for doped Mott insulators, *Europhysics Letters (EPL)* **70**, 492 (2005).
 - [32] E. Jeckelmann, Ground-state phase diagram of a half-filled one-dimensional extended Hubbard model, *Phys. Rev. Lett.* **89**, 236401 (2002).

- [33] E. Jeckelmann, Comment on “Accurate ground-state phase diagram of the one-dimensional extended Hubbard model at half filling”, Phys. Rev. B **71**, 197101 (2005).
- [34] S. Ejima and S. Nishimoto, Phase diagram of the one-dimensional half-filled extended Hubbard model, Phys. Rev. Lett. **99**, 216403 (2007).
- [35] C. Mund, Ö. Legeza, and R. M. Noack, Quantum information analysis of the phase diagram of the half-filled extended Hubbard model, Phys. Rev. B **79**, 245130 (2009).
- [36] N. S. Sariciftci, *Primary Photoexcitations in Conjugated Polymers: Molecular Exciton Versus Semiconductor Band Model* (World Scientific, 1998).
- [37] M. Schott, Optical properties of single conjugated polymer chains (polydiacetylenes), in *Photophysics of Molecular Materials* (John Wiley & Sons, Ltd, 2005) Chap. 3, pp. 49–151.
- [38] C. S. Yannoni and T. C. Clarke, Molecular geometry of cis- and trans-polyacetylene by nutation NMR spectroscopy, Phys. Rev. Lett. **51**, 1191 (1983).
- [39] M. Duijvestijn, A. Manenschijn, J. Smidt, and R. Wind, Structural information of undoped trans-polyacetylene obtained by ^{13}C 2d NMR combined with dynamic nuclear polarization, Journal of Magnetic Resonance (1969) **64**, 461 (1985).
- [40] D. Baeriswyl, D. K. Campbell, and S. Mazumdar, An overview of the theory of π -conjugated polymers, in *Conjugated Conducting Polymers*, Springer Series in Solid-State Sciences **102**, edited by H. G. Kiess (Springer, Berlin, Heidelberg, 1992) pp. 7–133.
- [41] W. Barford, *Electronic and optical properties of conjugated polymers*, International series of monographs on physics **129** (Clarendon Press, Oxford, UK, 2005).
- [42] G. Barcza, W. Barford, F. Gebhard, and O. Legeza, Excited states in polydiacetylene chains: A density matrix renormalization group study, Phys. Rev. B **87**, 245116 (2013).
- [43] N. Schuch, J. I. Cirac, and M. M. Wolf, Quantum states on harmonic lattices, Comm. Math. Phys. **267**, 65 (2006).
- [44] G. S. Uhrig and R. Vlamings, Inhibition of phase separation and appearance of new phases for interacting spinless fermions, Phys. Rev. Lett. **71**, 271 (1993).
- [45] A. Georges, G. Kotliar, W. Krauth, and M. J. Rozenberg, Dynamical mean-field theory of strongly correlated fermion systems and the limit of infinite dimensions, Rev. Mod. Phys. **68**, 13 (1996).
- [46] Q. Si and J. L. Smith, Kosterlitz-Thouless Transition and Short Range Spatial Correlations in an Extended Hubbard Model, Phys. Rev. Lett. **77**, 3391 (1996).